



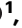





ATP dynamics as a predictor of future podocyte structure and function after acute ischemic kidney injury in female mice

Received: 10 February 2023

Accepted: 4 November 2024

Published online: 22 November 2024

 Check for updates

Masahiro Takahashi ¹, Shinya Yamamoto¹, Shigenori Yamamoto ^{1,2}, Akihiro Okubo ¹, Yasuaki Nakagawa³, Koichiro Kuwahara ⁴, Taiji Matsusaka ⁵, Shingo Fukuma ^{6,7}, Masamichi Yamamoto^{1,8}, Michiyuki Matsuda ^{9,10,11} & Motoko Yanagita ^{1,2} ✉

Acute kidney injury (AKI), typically caused by ischemia, is a common clinical complication with a poor prognosis. Although proteinuria is an important prognostic indicator of AKI, the underlying causal mechanism remains unclear. In vitro studies suggest that podocytes have high ATP demands to maintain their structure and function, however, analyzing their ATP dynamics in living kidneys has been technically challenging. Here, using intravital imaging to visualize a FRET-based ATP biosensor expressed systemically in female mice due to their suitability for glomerular imaging, we monitor the in vivo ATP dynamics in podocytes during ischemia reperfusion injury. ATP levels decrease during ischemia, but recover after reperfusion in podocytes, exhibiting better recovery than in glomerular endothelial cells. However, prolonged ischemia results in insufficient ATP recovery in podocytes, which is inversely correlated with mitochondrial fragmentation and foot process effacement during the chronic phase. Furthermore, preventing mitochondrial fission via pharmacological inhibition ameliorates podocyte injury in vitro, ex vivo, and in vivo. Thus, these findings provide several insights into how ATP depletion and mitochondrial fragmentation contribute to podocyte injury after ischemic AKI and could potentially be therapeutic targets.

Acute kidney injury (AKI), frequently caused by ischemia^{1,2}, is a common clinical condition associated with high morbidity and mortality^{3,4}. Although excessive proteins in urine or proteinuria -due to defects in the glomerular filtration barrier- is known to be a consequence of AKI^{5,6} and persisting proteinuria after AKI is associated with worse renal

prognosis⁷, whether glomerular injury contributes to the pathophysiology underlying ischemic AKI remains unclear.

The glomerular filtration barrier is composed of glomerular endothelial cells, glomerular basement membrane, and highly differentiated cells, called podocytes, with podocytes playing the most

¹Department of Nephrology, Graduate School of Medicine, Kyoto University, Kyoto, Japan. ²Institute for the Advanced Study of Human Biology, Kyoto University, Kyoto, Japan. ³Department of Cardiovascular Medicine, Graduate School of Medicine, Kyoto University, Kyoto, Japan. ⁴Department of Cardiovascular Medicine, Shinshu University School of Medicine, Matsumoto, Japan. ⁵Institute of Medical Science and Department of Physiology, Tokai University School of Medicine, Isehara, Japan. ⁶Human Health Sciences, Graduate School of Medicine, Kyoto University, Kyoto, Japan. ⁷Department of Epidemiology Infectious Disease Control and Prevention, Hiroshima University Graduate School of Biomedical and Health Sciences, Hiroshima, Japan. ⁸National Cerebral and Cardiovascular Center Research Institute, Osaka, Japan. ⁹Laboratory of Biomedicine and Cell Signaling, Graduate School of Biostudies, Kyoto University, Kyoto, Japan. ¹⁰Department of Pathology and Biology of Diseases, Graduate School of Medicine, Kyoto University, Kyoto, Japan. ¹¹Institute for Integrated Cell-Material Sciences, Kyoto University, Kyoto, Japan. ✉e-mail: motoy@kuhp.kyoto-u.ac.jp

important role in its barrier function. Podocytes possess interdigitating foot processes, that are supported by an elaborate network of actin cytoskeleton⁸. As actin cytoskeletal networks require adenosine 5' triphosphate (ATP) for its polymerization, this suggests that differentiated podocytes are likely to require a stable energy supply as well as functional mitochondria to produce such energy, in order to maintain structural and functional integrity in their foot processes⁹. In support of this, cultured podocytes increase their ATP content by up to 80% during differentiation by generating a robust mitochondrial networks and by upregulating glycolytic enzymes to match the increasing energy demand¹⁰. Furthermore, patients with mutations in mitochondrial genes or in the coenzyme Q₁₀ (CoQ₁₀) synthetic pathway have been shown to display signs of podocyte injury and proteinuria¹¹. Together, this suggests that mitochondrial injury and changes in podocyte energy metabolism may lead to glomerular injury that results in proteinuria after ischemic AKI. However, direct evidence has been lacking due to the technical difficulties of determining intracellular ATP in glomeruli of kidneys in vivo.

Here, we used an intravital imaging technique and Förster resonance energy transfer (FRET)-based ATP biosensor mice to assess the energy dynamics in podocytes during ischemia reperfusion injury (IRI). We show not only that ATP dynamics in acute phase can act as a readout for long-term structural changes in podocytes but also demonstrate that pharmacological inhibition of mitochondrial fission in podocytes in vitro and in vivo may be a potential clinical strategy for preventing proteinuria and glomerular injury during ischemic AKI.

Results

Prolonged ischemia induces podocyte injury and proteinuria

To determine the effects of ischemia on podocytes in vivo, we first evaluated mice treated with either 30-min or 45-min of ischemia. We observed prominent podocyte foot process effacement in mice treated with 45-min of ischemia on day 14, with 55.0% of glomeruli exhibiting an increased foot process width (Fig. 1A–C). However, these effects on foot process effacement were not observed in mice treated with 30-min of ischemia, and only 12.9% of glomeruli showed an increase in foot process width (Fig. 1A–C). Furthermore, while the numbers of podocytes in glomeruli were comparable between the sham and 45-min ischemia groups (Fig. 1D, E), immunostaining revealed reduced expression of podocin, nephrin, and nestin after 45 min of ischemia (Fig. 1D, F). An increase in the urinary albumin-to-creatinine ratio (ACR) from injured kidneys was observed in the urine collected on day 7–8, day 14–15, and day 28–29 after 45-min IRI (Fig. 1G, H). We also observed sustained foot process effacement on day 29 after 45-min IRI (Fig. 1I, J). Additionally, some glomeruli showed shrinkage of capillary tufts and sclerotic changes on day 29 after IRI (Supplementary Fig. 1), which resemble features of ischemic glomeruli in chronic phase after kidney transplantation¹². These results suggest that prolonged exposure to ischemia leads to podocyte injury and defects in glomerular filtration barrier function even up to four weeks after IRI.

Intravital ATP imaging of mouse glomeruli during ischemia

Next, to visualize ATP levels in glomeruli, we used GO-ATeam2 mice that systemically express a FRET-based ATP biosensor GO-ATeam2¹³, which uses variants of green fluorescent protein (GFP) and kusabira orange fluorescent protein (OPF) to sandwich the ϵ -subunit of *Bacillus subtilis* F₀F₁-ATP synthase¹⁴. As the ϵ -subunit binds specifically to ATP but not to ADP, dATP, or GTP, it allows ATP levels to be quantitatively determined using OPF/GFP ratios (ATP^{ratio}), which have a linear correlation with cellular ATP concentrations at a high specificity¹⁴. Previously, we established an ATP imaging technique for living kidneys using multi-photon microscopy to analyze ATP dynamics of proximal and distal tubules during renal ischemia in male GO-ATeam2 mice¹⁵. However, we were unable to monitor glomerular ATP dynamics, likely

due to the thickness of the kidney cortex. To overcome these difficulties, we focused only on female mice that have a thinner kidney cortex compared to males to observe glomeruli. Indeed, we were able to observe from the surface of female GO-ATeam2 mouse kidneys, the proximal tubules, distal tubules, collecting ducts (16 μ m deep; Fig. 2A) and glomeruli (40 μ m deep; Fig. 2B). In Go-ATeam2 mice, the expression of the biosensor is under control of the CAG promoter inserted in the ROSA26 locus¹⁶. The expression of CAG promoter has been previously reported to be heterogenous in several organs including the kidney, as well as among different cell types¹⁷. The cells located at the periphery of glomeruli showed strong fluorescence (Fig. 2C) and were identified as podocytes by immunostaining (Fig. 2D). ATP^{ratio} of podocytes was analyzed in single cell level by manual segmentation (Supplementary Fig. 2A). The average ATP^{ratio} of podocytes was 2.36, and the inter-glomerular variation of the podocyte ATP^{ratio} was relatively small compared to those of other segments (Fig. 2E). By measuring ATP^{ratio} in primary cultured MEFs expressing GO-ATeam2 with arbitrary intracellular ATP concentrations, we estimated actual ATP concentrations of kidney cells in vivo (Supplementary Fig. 2B, C). Intracellular ATP concentrations of kidney cells ranged from 3 mM to 4.2 mM (Supplementary Fig. 2D).

To investigate how ATP dynamics in glomeruli are affected during ischemia, we performed time-lapse imaging. First, we focused on the variation of overall ATP change between glomeruli before dissecting cell-type specific ATP dynamics. Upon ischemia induction, the ATP levels in the glomeruli gradually decreased (Fig. 3A). While the ATP reduction rates in distal tubules and collecting ducts varied between tubules¹⁵, those in glomeruli were relatively uniform. Magnified views of podocytes showed a gradual decrease in ATP^{ratio} after ischemia induction, reaching nadir levels in about 20 min (Fig. 3B, C). GO-ATeam2 mice that underwent sham surgery did not show any decrease in podocyte ATP, therefore suggesting negligible photo-toxicity or photo-bleaching effects with our experimental set-up (Fig. 3B, C). We also compared ATP dynamics during ischemia between podocytes and other nephron segments. While the ATP^{ratio} in proximal tubules quickly decreased within 2 min after ischemia induction, that of distal tubules and collecting ducts reduced only gradually and reached nadir levels in about 25 min and 45 min, respectively (Fig. 3D, E). This indicates that the ischemia-induced decrease in ATP in podocytes was much slower than that in proximal tubules, similar to that in distal tubules, but faster than that in collecting ducts.

ATP recovery in podocytes following reperfusion is insufficient after prolonged ischemia

We then analyzed ATP dynamics in podocytes during reperfusion after ischemia. Podocytes showed a slightly delayed ATP recovery after prolonged ischemia (Fig. 4A–C, and Supplementary Fig. 3), displaying similar effects to the proximal tubules, which we previously reported¹⁵. After initial recovery of ATP, the podocyte ATP^{ratio} reached stable levels, which were lower than the pre-ischemia levels, during 30 min of reperfusion (Fig. 4A, B, and Supplementary Fig. 3). ATP % recovery of podocytes after 30 min of reperfusion showed an ischemic time-dependent decrease (Fig. 4D). This indicates that the ATP recovery in podocytes after prolonged ischemia was insufficient.

Intra-glomerular heterogeneity of ATP dynamics during IRI

Interestingly, in our analysis, we observed heterogeneity in ATP dynamics among glomerular cells. Compared to podocytes, cells positioned inside the glomerular tufts showed slower reduction of ATP during ischemia (Fig. 5A, B). Upon reperfusion, we found a group of cells with lower ATP levels than the surrounding cells (Fig. 5C). Based on their location in the glomerulus and the relatively low biosensor expression (Fig. 2D), we reasoned that they were not podocytes but potentially either endothelial cells or mesangial cells.

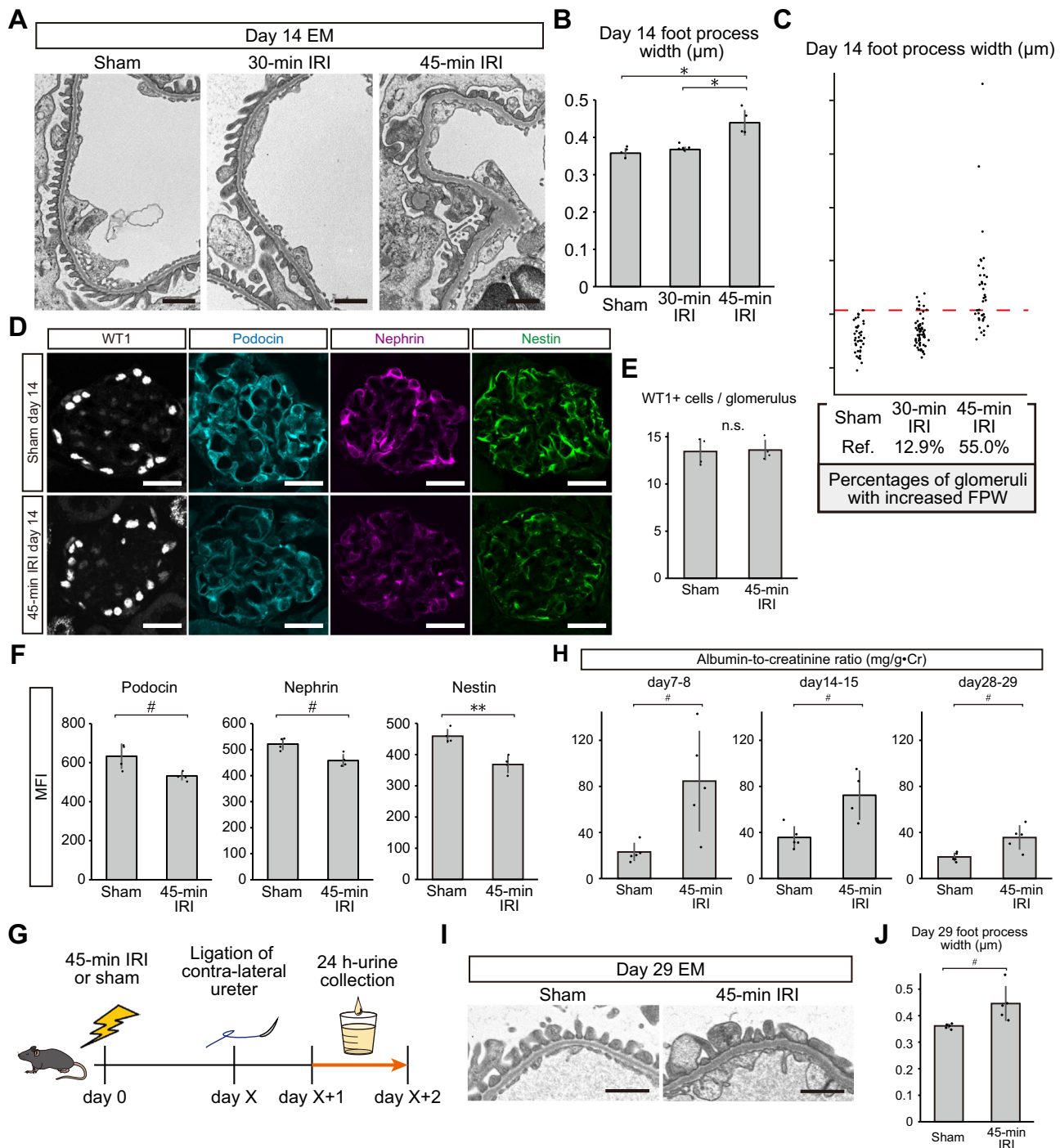


Fig. 1 | Pathological changes in podocytes and albuminuria after ischemia reperfusion injury (IRI). **A** Electron microscopy images of glomerular tufts 14 days after 30-min IRI, 45-min IRI, and sham surgery. **B** Podocyte foot process widths after each condition. Each dot represents the average foot process width of at least five glomeruli from each mouse. Exact *p*-values: Sham vs 45-min IRI: **p* = 0.0003; 30-min IRI vs 45-min IRI: **p* = 0.0005. **C** Percentages of glomeruli with an increased foot process width. Each dot represents the foot process width for each glomerulus. The dashed red line indicates the threshold of the normal foot process width defined as the largest foot process width in the sham surgery group. **D** Podocyte marker protein immunostaining (WT1, podocin, nephrin, and nestin) 14 days after 45-min IRI or sham surgery. **E** The number of WT1-positive cells per glomerulus after 45-min IRI or sham surgery. Exact *p*-value: *p* = 0.8623. **F** The mean fluorescence

intensity (MFI) of podocin, nephrin, and nestin 14 days after 45-min IRI or sham surgery. Exact *p*-values: Podocin: #*p* = 0.0477; Nephrin: #*p* = 0.0100; Nestin: ***p* = 0.0027. **G** Graphical representation of the albumin-to-creatinine ratios (ACR) measurement in the urine from injured kidneys. **H** ACR on day 7–8, day 14–15, and day 28–29 after IRI or sham surgery. Exact *p*-value: day 7–8: #*p* = 0.0336; day 14–15: #*p* = 0.0346; day 28–29: #*p* = 0.0206. **I** Electron microscopy images of glomerular tufts 29 days after 45-min IRI and sham surgery. **J** Podocyte foot process widths 29 days after 45-min IRI and sham surgery. Exact *p*-value: #*p* = 0.0450. **p* < 0.001; ***p* < 0.01; #*p* < 0.05. Scale bars: 1 μm in (**A** and **I**) and 20 μm in (**D**). EM, electron microscopy; IRI, ischemia reperfusion injury; FPW, foot process width; MFI, mean fluorescence intensity; n.s., not significant.

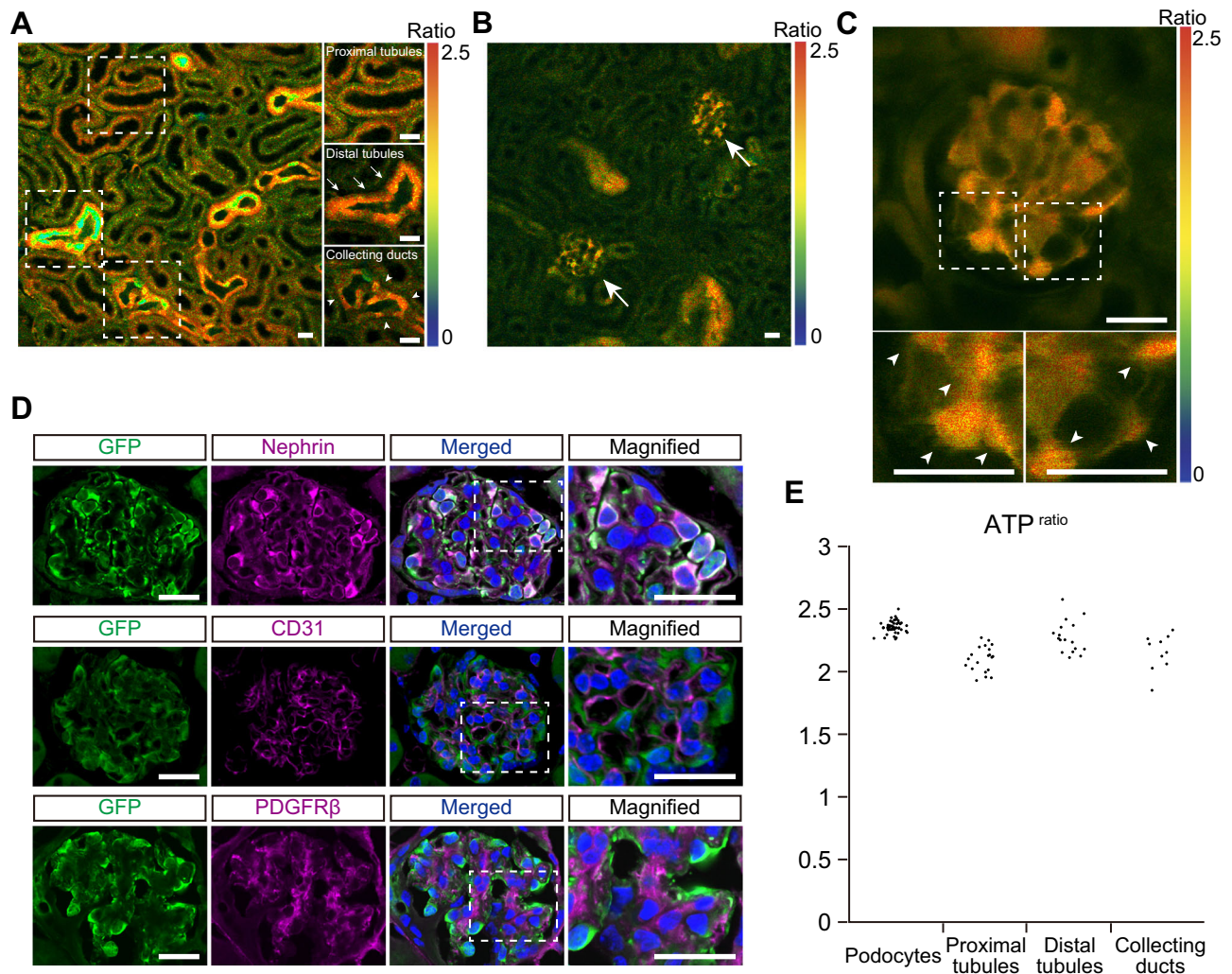


Fig. 2 | ATP imaging of the glomeruli and tubules in the living kidneys. **A** A representative ATP image of the renal cortex (16 μm deep from the kidney surface). Magnified and laser-adjusted images of the proximal tubules, distal tubules, and collecting ducts are shown in the right panels. **B** A representative ATP image of the renal cortex containing glomeruli (40 μm deep from the kidney surface). Arrows indicate glomeruli. **C** A magnified ATP image of a glomerulus. Areas in the dashed boxes are magnified in lower panels. Arrowheads in the lower panels indicate podocytes. **D** Immunostaining of GO-ATeam2 biosensor and markers in glomerular cells in GO-ATeam2 mice. The GO-ATeam2 biosensor was labelled via GFP

immunostaining. The top, middle, and bottom panels show double staining of the biosensor and marker proteins in podocytes (nephrin), endothelial cells (CD31), and mesangial cells (PDGFRβ), respectively. Areas in the dashed boxes are magnified in right panels. **E** Variation of the ATP^{ratio} in podocytes, proximal tubules, distal tubules, and collecting ducts. Each dot represents the average podocyte ATP^{ratio} in each glomerulus or tubular ATP^{ratio} for each section. The average ATP^{ratio} of podocytes, proximal tubules, distal tubules, and collecting ducts was 2.36 ± 0.05, 2.11 ± 0.10, 2.32 ± 0.11, and 2.15 ± 0.10, respectively. Scale bars: 20 μm in (A, B, C, and D).

To identify cell type-specific ATP dynamics among glomerular cells during IRI, *Nphs1*-Cre mice and *Tie2*-Cre mice were bred with GO-ATeam2^{fllox/+} mice to generate mice expressing GO-ATeam2 specifically in podocytes or endothelial cells, respectively (*Nphs1*-ATeam and *Tie2*-ATeam mice). Cell type-specific expression of the GO-ATeam2 biosensor was validated by co-localization with cell type-specific markers (Supplementary Fig. 4A–D), which enables cell-type specific ATP^{ratio} measurement (Supplementary Fig. 4E, F). Using *Nphs1*-ATeam and *Tie2*-ATeam mice, we visualized cell type-specific ATP dynamics during ischemia reperfusion and found that the decrease in ATP in endothelial cells occurred as fast as that in podocytes during ischemia (Fig. 5D, E), suggesting that the cells with slow ATP decline during ischemia in the systemic GO-ATeam2 mice (Fig. 5A, B) were unlikely to be endothelial cells. Upon reperfusion, *Nphs1*-ATeam mice and *Tie2*-ATeam mice showed different ATP recovery patterns in podocytes and endothelial cells (Fig. 5F, G), with ATP recovery in endothelial cells being worse than that in podocytes (Fig. 5F, G, H).

Although a previous in vitro study showed that lamellipodia of cultured podocytes are more dependent on glycolytic ATP production compared with mitochondria-rich perinuclear cytoplasm¹⁸, we observed no such differences in ATP levels between the cell body, the major processes, and the secondary processes of podocytes (Supplementary Fig. 5).

Mitochondrial fragmentation in podocytes in the super-acute phase of IRI

To analyze pathological changes in podocytes in the super-acute phase (30 min after reperfusion) of IRI, transmission electron microscopy (TEM) was performed. Foot process effacement of podocytes was not observed in the super-acute phase after IRI (Fig. 6A, B). However, round and short mitochondria increased in podocytes, especially after long ischemia, potentially indicating mitochondrial fragmentation (Fig. 6A, C, and Supplementary Fig. 6A). Three-dimensional analysis of podocyte microstructures clearly showed fragmentation of mitochondria and disruption of

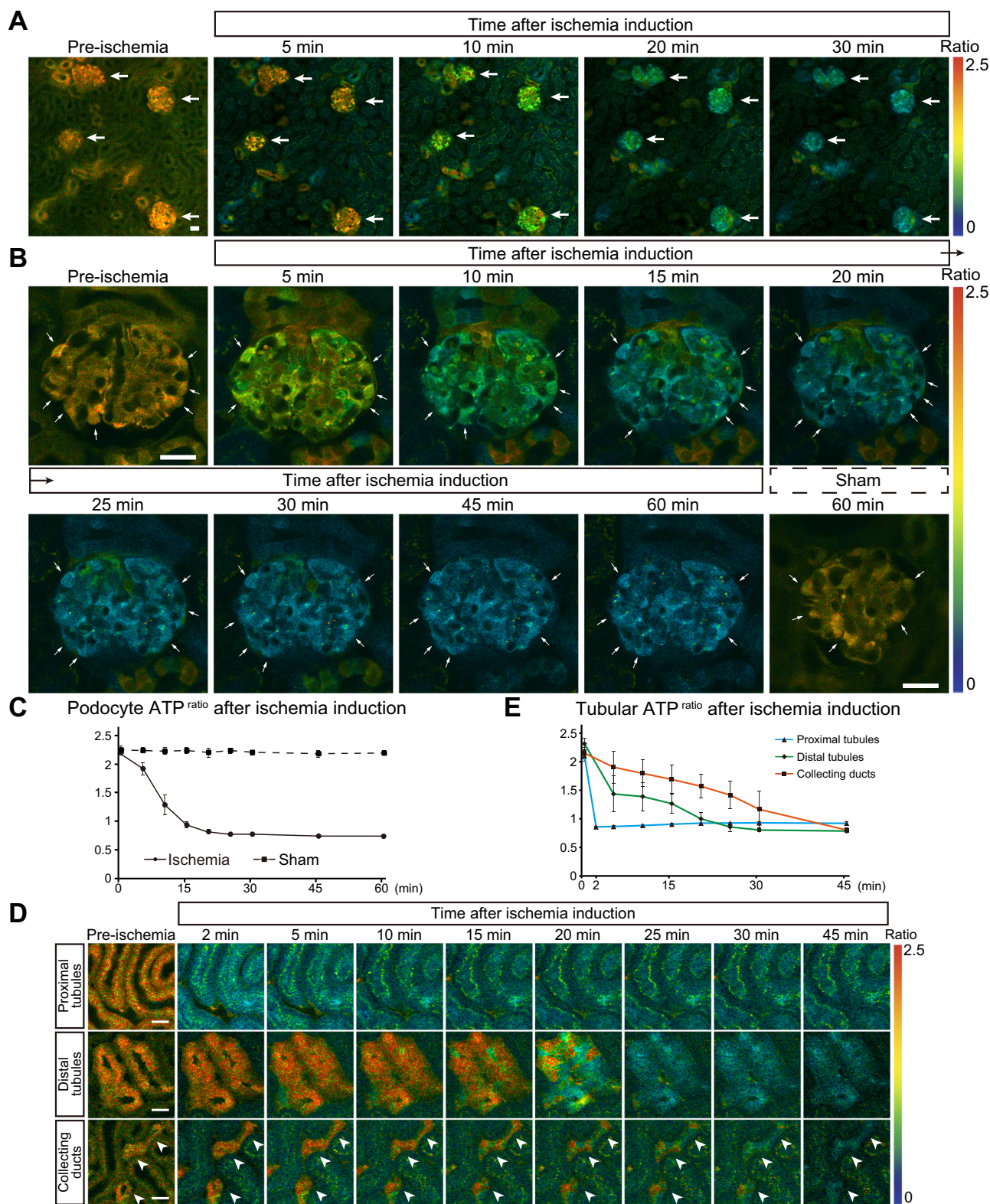


Fig. 3 | Podocyte ATP levels decrease gradually after ischemia induction. **A** ATP images of the kidney cortex before and after ischemia induction. Arrows indicate glomeruli. **B** Magnified ATP images of a glomerulus before and after ischemia induction or sham operation. Arrows indicate podocytes. **C** Quantification of podocyte ATP^{ratio} after induction of ischemia (continuous line) or sham operation

(dashed line). **D** Magnified ATP images focusing on proximal tubules, distal tubules, and collecting ducts before and after ischemia induction. Collecting ducts are indicated by white arrowheads. **E** Quantification of the ATP^{ratio} in proximal tubules (S1 segment), distal tubules, and collecting ducts during ischemia. Scale bars: 20 μ m in (**A**, **B**, and **D**).

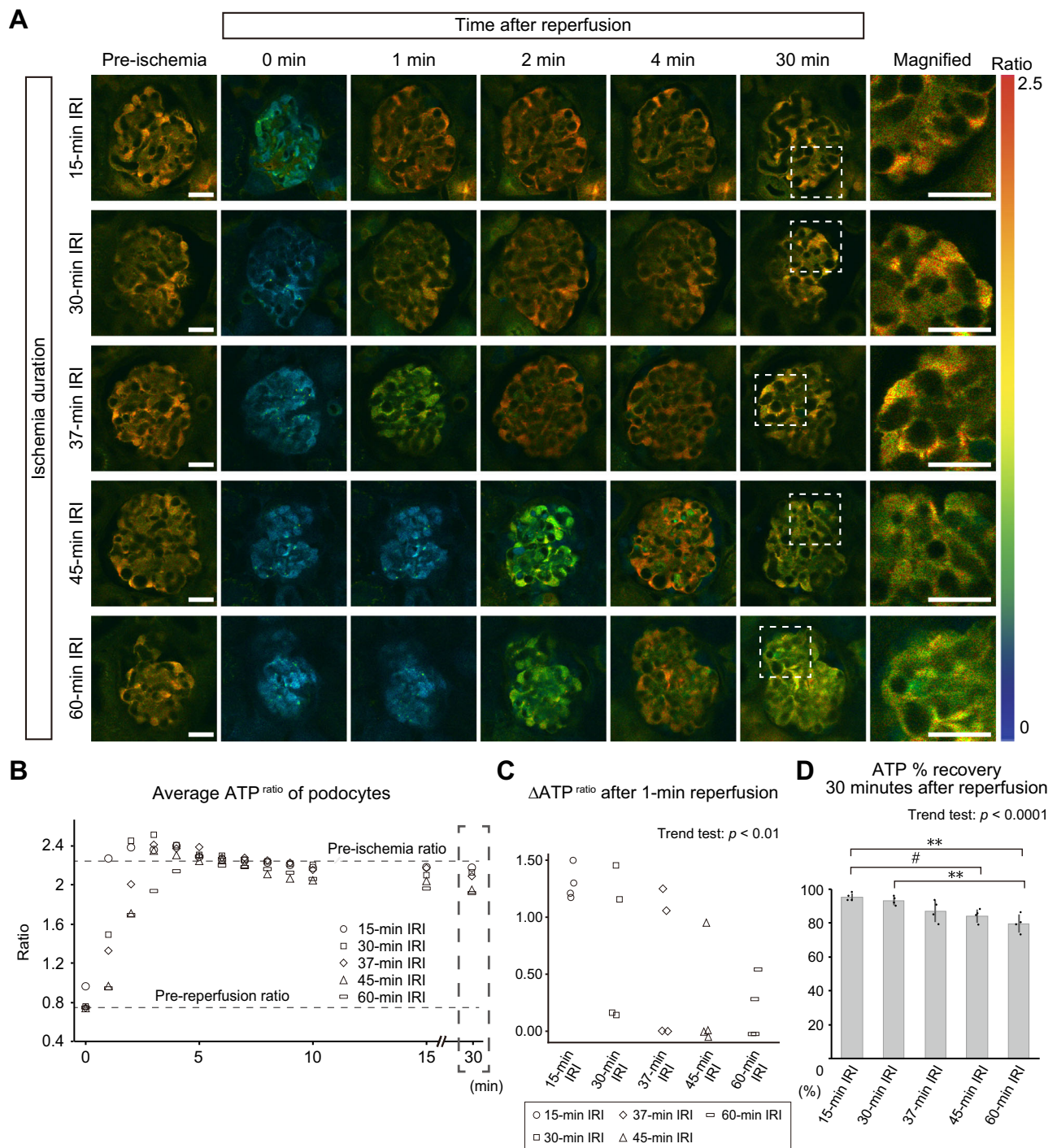


Fig. 4 | ATP recovery after ischemia reperfusion in podocytes is delayed and insufficient after prolonged ischemia. **A** ATP images of glomeruli before and after ischemia reperfusion. Magnified images of glomeruli 30 min after reperfusion are shown in the right panels. **B** Quantification of the podocyte ATP^{ratio} after reperfusion. The average of basal ATP^{ratio} before ischemia and the lowest ATP^{ratio} before reperfusion in all groups are indicated by dashed lines. The mean ATP^{ratio}s after different ischemic times are shown separately in Supplementary Fig. 2. **C** Changes

of the ATP^{ratio} in 1 min after reperfusion. Exact p -value: $p = 0.0010$. **D** ATP % recovery after reperfusion. ATP % recovery was defined based on the basal ATP^{ratio} before ischemia and the lowest ATP^{ratio} before reperfusion (see “Methods” for the detailed information). Exact p -value: 15-min IRI vs 45-min IRI: $\#p = 0.0218$; 15-min IRI vs 60-min IRI: $**p = 0.0013$; 30-min IRI vs 60-min IRI: $**p = 0.0047$. $p < 0.0001$ for the trend test. $**p < 0.01$; $\#p < 0.05$. Scale bars: 20 μ m in A. IRI, ischemia reperfusion injury.

their continuity after IRI (Fig. 6D and Supplementary Movies 1–6). Immunostaining showed early increase in DRP1 protein, a key component of mitochondrial fission machinery, in podocytes after ischemia reperfusion (Supplementary Fig. 6B). These results suggest that mitochondrial fragmentation is an early indicator of podocyte injury in the super-acute phase of IRI.

ATP recovery in the super-acute phase predicts morphological changes of podocytes in the chronic phase of IRI

TEM images of GO-ATeam2 mice 14 days after IRI revealed prominent foot process effacement and mitochondrial fragmentation in podocytes after 45- and 60-min of ischemia, whereas these changes were not obvious in podocytes after short ischemia (Fig. 7A–C, and

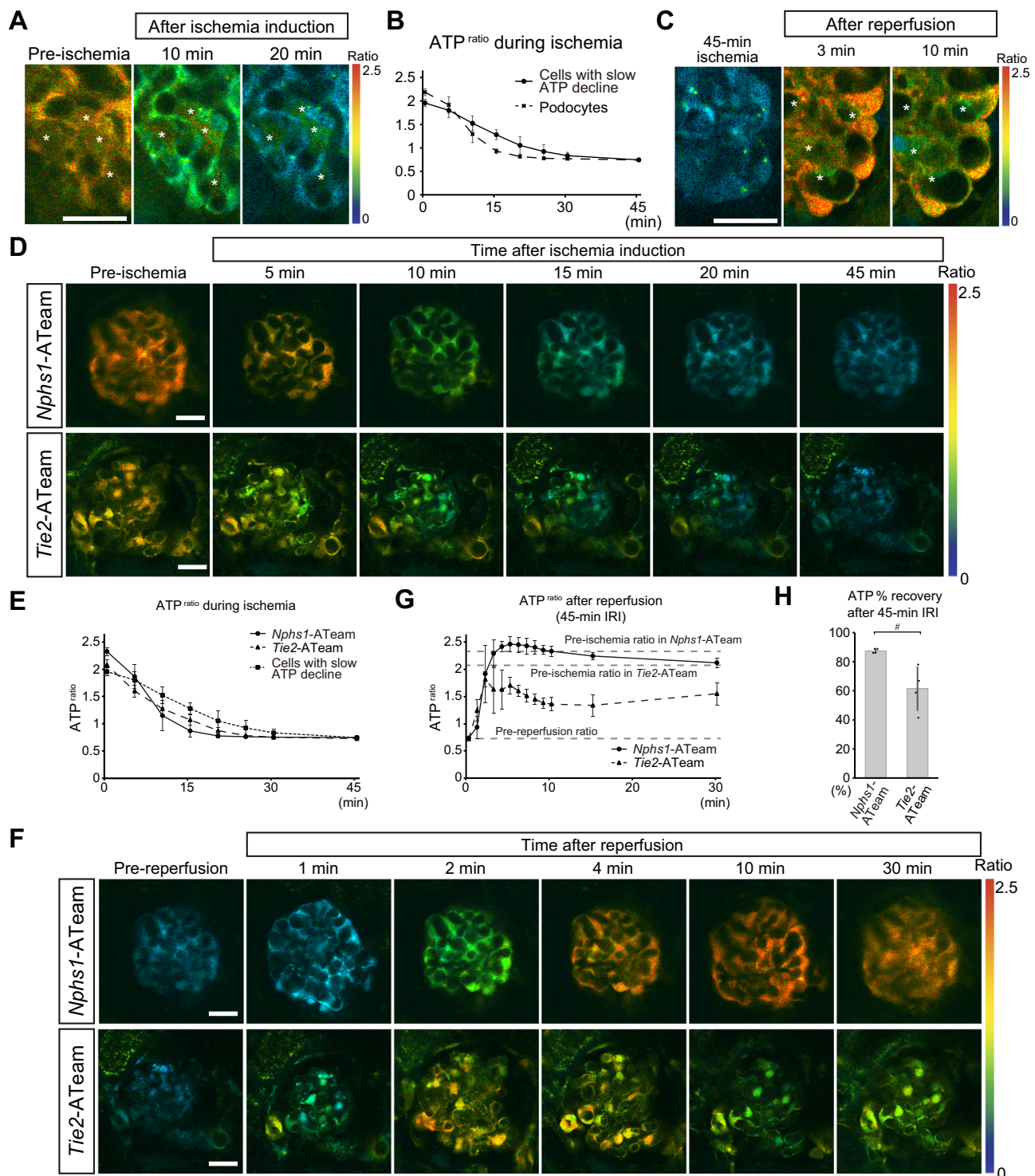


Fig. 5 | Intra-glomerular heterogeneity of ATP dynamics during ischemia and reperfusion. **A** Magnified ATP images of a glomerulus from GO-A_{Team}2 mice before ischemia and after 10- and 20-min ischemia. Asterisks indicate a group of cells that maintained ATP levels better than the surrounding cells during ischemia. **B** Quantification of the ATP^{ratio} in the cells that showed the slower decrease in ATP during ischemia (represented by cells indicated by asterisks in **A**). For comparison, podocyte ATP^{ratio} is shown by a dashed line (data from Fig. 3C). **C** Magnified ATP images of a glomerulus from GO-A_{Team}2 mice during reperfusion after 45-min ischemia. Asterisks indicate a group of cells that showed hampered ATP recovery after reperfusion. **D** Representative ATP images of glomeruli from *Nphs1-ATeam*

and *Tie2-ATeam* mice during ischemia. **E** Quantification of the ATP^{ratio} in the glomeruli from *Nphs1-ATeam* and *Tie2-ATeam* mice during ischemia. Data in **(B)** was shown again for comparison. **F** Representative ATP images of glomeruli from *Nphs1-ATeam* and *Tie2-ATeam* mice after reperfusion. **G** Quantification of the ATP^{ratio} in glomeruli from *Nphs1-ATeam* mice and *Tie2-ATeam* mice after 45-min ischemia reperfusion. The basal ATP^{ratio} before ischemia in each group and the lowest ATP^{ratio} before reperfusion are indicated by dashed lines. **H** ATP % recovery in *Nphs1-ATeam* or *Tie2-ATeam* mouse glomeruli after 30-min reperfusion. Exact p -value: # $p = 0.0416$. # $p < 0.05$. Scale bars: 20 μ m in **(A, C, D, and F)**. IRI, ischemia reperfusion injury.

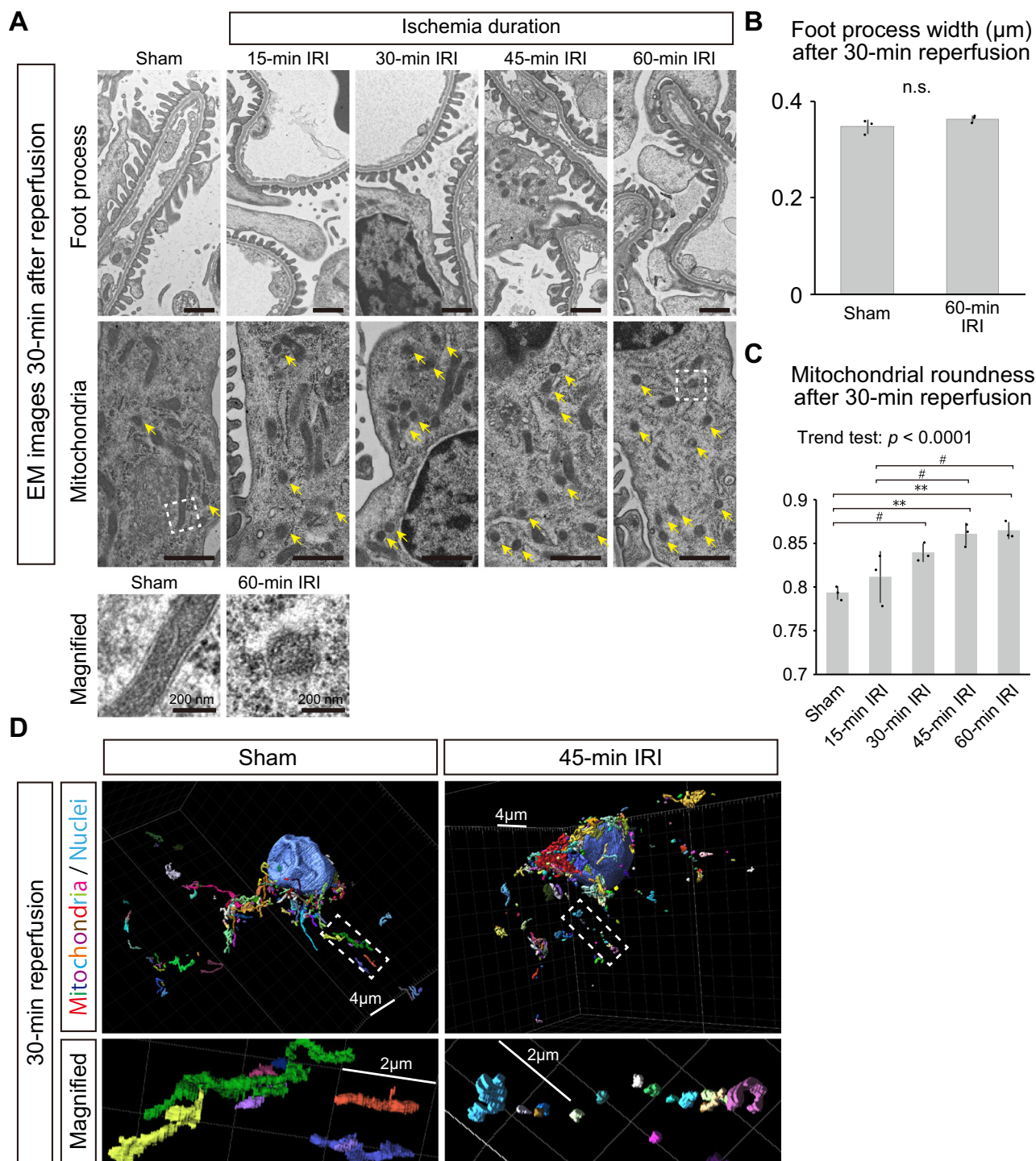
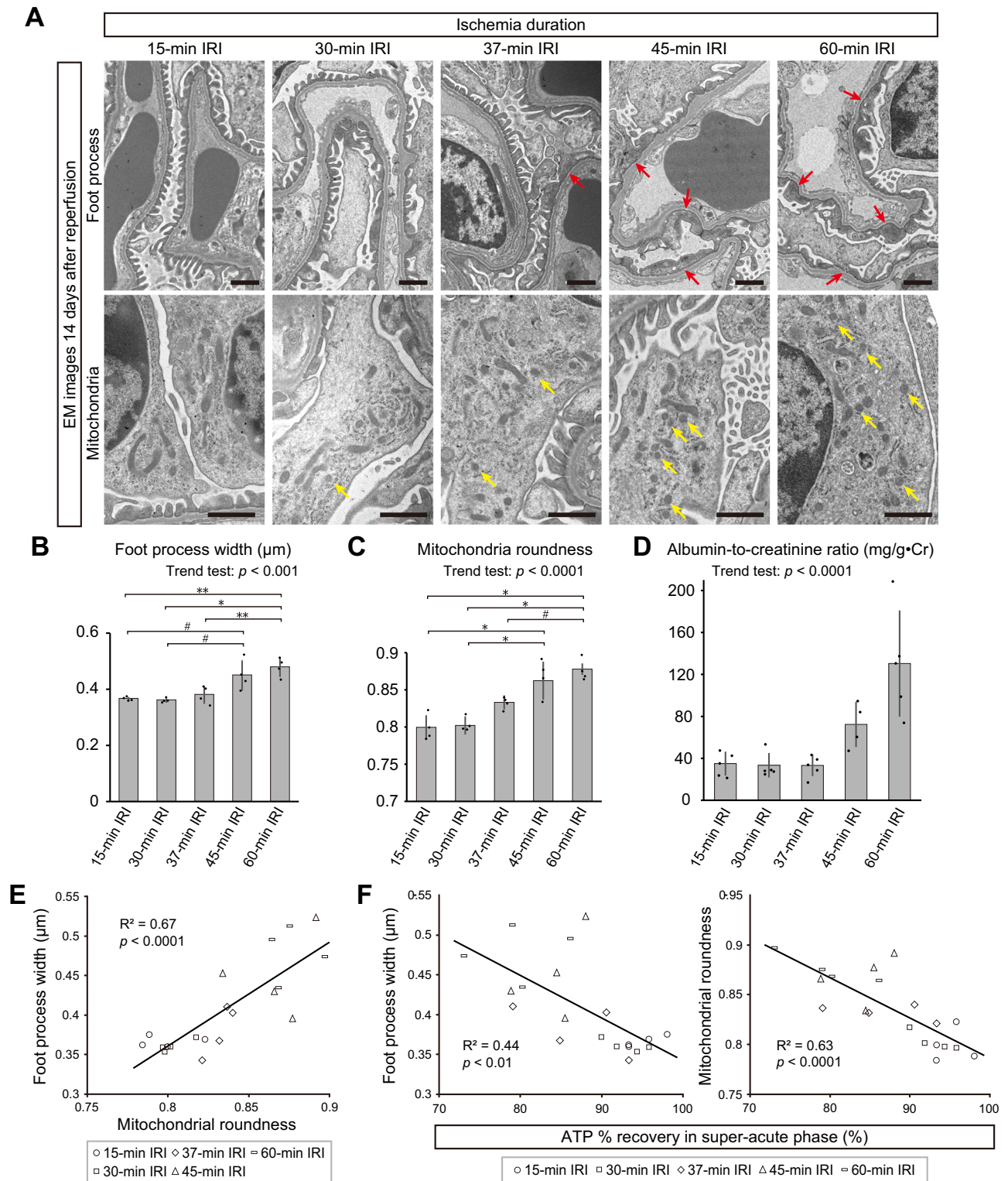


Fig. 6 | Mitochondrial fragmentation in podocytes in the super-acute phase of IRI. **A** Electron microscopic images of podocytes after 30-min reperfusion following 15-, 30-, 45-, or 60-min ischemia or sham surgery. Upper panels and lower panels focus on foot processes and mitochondria of podocytes, respectively. Yellow arrows indicate short and round-shaped mitochondria, which suggest mitochondrial fragmentation. Images below the main panels show magnified views of representative mitochondria in non-ischemia and ischemia groups. Wider views of electron microscopic images are shown in Supplementary Fig. 5A. **B** Quantitative analysis of the foot process width after sham surgery and 60-min IRI. Exact p -value: $p = 0.1989$. **C** Mitochondrial roundness after sham surgery and ischemia. Exact

p -value: Sham vs 30-min IRI: $\#p = 0.0376$; Sham vs 45-min IRI: $**p = 0.0034$; Sham vs 60-min IRI: $**p = 0.0022$; 15-min IRI vs 45-min IRI: $\#p = 0.0262$; 15-min IRI vs 60-min IRI: $\#p = 0.0164$. $p < 0.0001$ for the trend test. **D** Representative three-dimensional images of podocyte mitochondria after 30-min reperfusion following 45-min ischemia or sham surgery. For the rainbow colors, switching of colors indicates breaks of mitochondria. The large blue oval structures indicate nuclei. Magnified views focusing on mitochondria locating in cellular processes are shown below. Each box on a grid is $2 \mu\text{m}$ long. $**p < 0.01$; $\#p < 0.05$. Scale bars: $1 \mu\text{m}$ in (A), 200 nm in magnified images of (A), $4 \mu\text{m}$ in (D), $2 \mu\text{m}$ in magnified images of (D). IRI, ischemia reperfusion injury; EM, electron microscopy; n.s., not significant.



Supplementary Fig. 7A). Experiments using wild-type mice also confirmed the increase in ACR after long ischemia 14 days after IRI (Fig. 7D). Despite significant ATP insufficiency in the super-acute phase (Fig. 5F, G, H), endothelial cells appeared generally normal. Signs of endothelial injury, such as loss of fenestration and splitting of glomerular basement membrane, were observed in only a few glomeruli in the 60-min ischemia group (Supplementary Fig. 7B), and capillary-thrombosis was not present. Interestingly, mitochondrial roundness in podocytes showed a strong correlation with their foot process width (Fig. 7D), suggesting that structural stability of podocytes is

strongly associated with mitochondrial morphology. Finally, we analyzed the correlation between ATP recovery in the super-acute phase and microstructural changes of podocytes in the chronic phase of IRI. Strikingly, the ATP % recovery in podocytes in the super-acute phase showed a significant inverse correlation with the foot process width and mitochondrial roundness of podocytes in the chronic phase, respectively (Fig. 7E). These results potentially suggest that IRI-induced foot process effacement may occur through mitochondrial damage and breakdown of ATP homeostasis.

Fig. 7 | ATP recovery in the acute phase is inversely correlated with podocyte injury in the chronic phase after IRI. **A** Electron microscopic images of podocytes 14 days after various IRI severity levels. Upper and lower panels focus on podocyte foot processes and mitochondria, respectively. Red and yellow arrows indicate foot process effacement and fragmented mitochondria, respectively. Wider views of electron microscopic images are shown in Supplementary Fig. 6A. **B** Foot process widths 14 days after various IRI severity levels. Exact p -value: 15-min IRI vs 45-min IRI: $\#p = 0.0163$; 15-min IRI vs 60-min IRI: $**p = 0.0014$; 30-min IRI vs 45-min IRI: $\#p = 0.0104$; 30-min IRI vs 60-min IRI: $*p = 0.0009$; 37-min IRI vs 60-min IRI: $**p = 0.0046$. $p = 0.0006$ for the trend test. **C** Mitochondrial roundness 14 days after various IRI severity levels. Exact p -value: 15-min IRI vs 45-min IRI: $*p = 0.0002$; 15-

min IRI vs 60-min IRI: $*p < 0.0001$; 30-min IRI vs 45-min IRI: $*p = 0.0004$; 30-min IRI vs 60-min IRI: $*p = 0.0001$; 37-min IRI vs 60-min IRI: $\#p = 0.0108$. $p < 0.0001$ for the trend test. **D** Albumin-to-creatinine ratio on day 14–15 after 15-min, 30-min, 37-min, 45-min, and 60-min IRI. Data of 45-min IRI group in Fig. 1H was shown again for comparison. Exact p -value: $p < 0.0001$. **E** Correlation between the foot process width and mitochondrial roundness 14 days after IRI. Exact p -value: $p < 0.0001$. **F** Correlation between the foot process width or mitochondrial roundness 14 days after IRI and ATP % recovery in podocytes in the super-acute phase of IRI. Exact p -value: Foot process width-ATP % recovery: $p = 0.0016$; Mitochondrial roundness-ATP % recovery: $p < 0.0001$. $*p < 0.001$; $**p < 0.01$; $\#p < 0.05$. Scale bars: 1 μm in A. IRI, ischemia reperfusion injury; EM, electron microscopy.

Suppression of mitochondrial fission ameliorates actin disarrangement in cultured podocytes

To determine the pathophysiological significance of ATP decrease and mitochondrial fragmentation in podocytes, we mimicked these conditions in cultured podocytes using oligomycin A and 2-deoxy-D-glucose, which inhibit mitochondrial ATP synthesis and the glycolytic pathway, respectively (Fig. 8A). Administration of these agents effectively induced mitochondrial fission and reduced the mitochondrial membrane potential in cultured podocyte cell line (Fig. 8B–D). We also employed primary cultured podocytes derived from wild type mice, and found similar results; mitochondrial fragmentation and reduced mitochondrial membrane potential after ATP depletion (Fig. 8E–G). One hour after discontinuing these reagents, cultured podocytes showed mitochondrial fragmentation, accompanied by the reduction in stress fiber formation and synaptopodin expression (Fig. 8H–J). To investigate the role of mitochondrial fragmentation in podocytes, we treated podocytes with Mdivi-1, a GTPase inhibitor that specifically inhibits the mitochondrial fission protein DRP1. Interestingly, the administration of Mdivi-1 attenuated mitochondrial fragmentation and restored the number of stress fiber-positive cells (Fig. 8H–J). Primary cultured podocytes showed the similar signs of injury after ATP depletion, which was attenuated by Mdivi-1 treatment (Fig. 8K–M).

To further demonstrate the participation of podocyte DRP1 in the pathological conditions, we knocked down *Drp1* in cultured podocytes. Knockdown mediated by siRNA targeting *Drp1* indeed reduced DRP1 protein levels in cultured podocytes (Fig. 9A, B). Importantly, *Drp1* knockdown ameliorated mitochondrial fragmentation as well as stress fiber loss in cultured podocytes after ATP depletion (Fig. 9C–E), suggesting that DRP1 plays a pivotal role in mitochondrial fragmentation and cytoskeletal disarrangement in podocytes after ATP depletion stress.

Pharmacological inhibition of DRP1 reduces mitochondrial fragmentation and foot process effacement of podocytes in vivo and in slice cultured kidney

Since cultured podocytes are inherently different from podocytes in vivo¹⁹, we confirmed the beneficial effects of suppressing mitochondrial fragmentation after ATP-depletion stress in vivo. We induced 45-min ischemia in female wild-type mice and treated them with daily intraperitoneal injection of Mdivi-1 (50 mg/kg) or control vehicle after ischemia reperfusion (Fig. 10A), and assessed podocyte microstructures in chronic phase (day14) of injury by electron microscopy. Mice treated with Mdivi-1 showed significantly reduced mitochondrial roundness and foot process width than vehicle-treated mice (Fig. 10B, C).

We also employed a newly established ex vivo IRI model²⁰ to minimize the potential influence of Mdivi-1 on adjacent injured tubules and hemodynamic changes after IRI (Fig. 10D). After 45 min deprivation of oxygen and energy resource and 4 h of recovery phase, podocytes in cultured kidney slices showed significant mitochondrial fission and foot process effacement (Fig. 10E, F). In contrast, glomeruli treated by Mdivi-1 showed mitigation of mitochondrial fission and foot process effacement in podocytes, strongly supporting the likelihood that

Mdivi-1 exerts a direct protective effect on podocytes (Fig. 10E, F). These results suggest that alleviating mitochondrial fragmentation is protective for the podocyte cytoskeleton after ATP-depletion stress in vitro, in ex vivo model, and in vivo.

Discussion

Previous work has implicated mitochondrial dysfunction in the proximal tubules in the pathophysiology underlying ischemic AKI^{15,21,22}, though the cause of proteinuria after ischemic AKI remained unclear. Mitochondrial dysfunction is also an important pathological feature in podocyte injury^{23–25}, however, investigations focusing on mitochondrial dysfunction of podocytes after AKI, especially in the IRI model, have not existed to date. Importantly, our study reveals podocyte ATP dynamics during ischemia reperfusion at a single cell resolution, demonstrating the link between podocyte ATP dynamics in the acute phase and podocyte structure and function in the chronic phase. Here, we have shed light on the pathophysiology of podocyte injury after IRI by showing that ATP depletion and mitochondrial injury in podocytes contribute to foot process effacement in the chronic phase of ischemic AKI.

ATP metabolism in podocytes has received much attention recently²⁶, however, assessing intracellular ATP in glomeruli has been technically challenging due to limitations in spatial-temporal resolution of conventional methods such as a luciferase assay, ³¹P nuclear magnetic resonance, and mass spectrometry imaging. Therefore most studies to-date have focused on cultured podocytes that are inherently different from podocytes in vivo¹⁹.

Multiphoton microscopy has served as a powerful tool to dissect pathophysiology in the living kidneys owing to its characteristic high spatial-temporal resolution and low invasiveness^{27–29}. Using these technical advantages, combined with GO-ATeam2 mice, here we provided several insights into ATP metabolism in podocytes during IRI. Firstly, we succeeded in visualizing the ATP dynamics in podocytes during ischemia and comparing them with those of other renal epithelia in the living kidneys. ATP decline in podocytes after ischemia was significantly slower than that in the proximal tubules, similar to that in the distal tubules, and faster than that in the collecting ducts. These differences in ATP dynamics might be at least partially due to different dependence on the glycolytic capacity and mitochondrial oxidative phosphorylation in each segment. The glycolytic capacity may work protectively in ischemia, however, mitochondria could paradoxically accelerate the decrease in ATP during ischemia. F₀/F₁ ATP synthase in the mitochondrial inner membrane produces large amount of ATP under the normal condition, but under conditions that collapse the mitochondrial membrane potential, it is suggested to take up and hydrolyze cytosolic ATP to maintain the membrane potential^{30–32}. While mitochondria-rich proximal tubules, which have limited ability of glycolysis^{33,34}, showed a rapid decrease in ATP during ischemia, a slower decrease in ATP in podocytes may reflect their substantial glycolytic capacity, which was shown in cultured podocytes^{10,18,35}. In the same way, potentially greater influence of mitochondrial ATP degradation in podocytes and distal tubules may explain the relatively faster ATP decline in these cell types

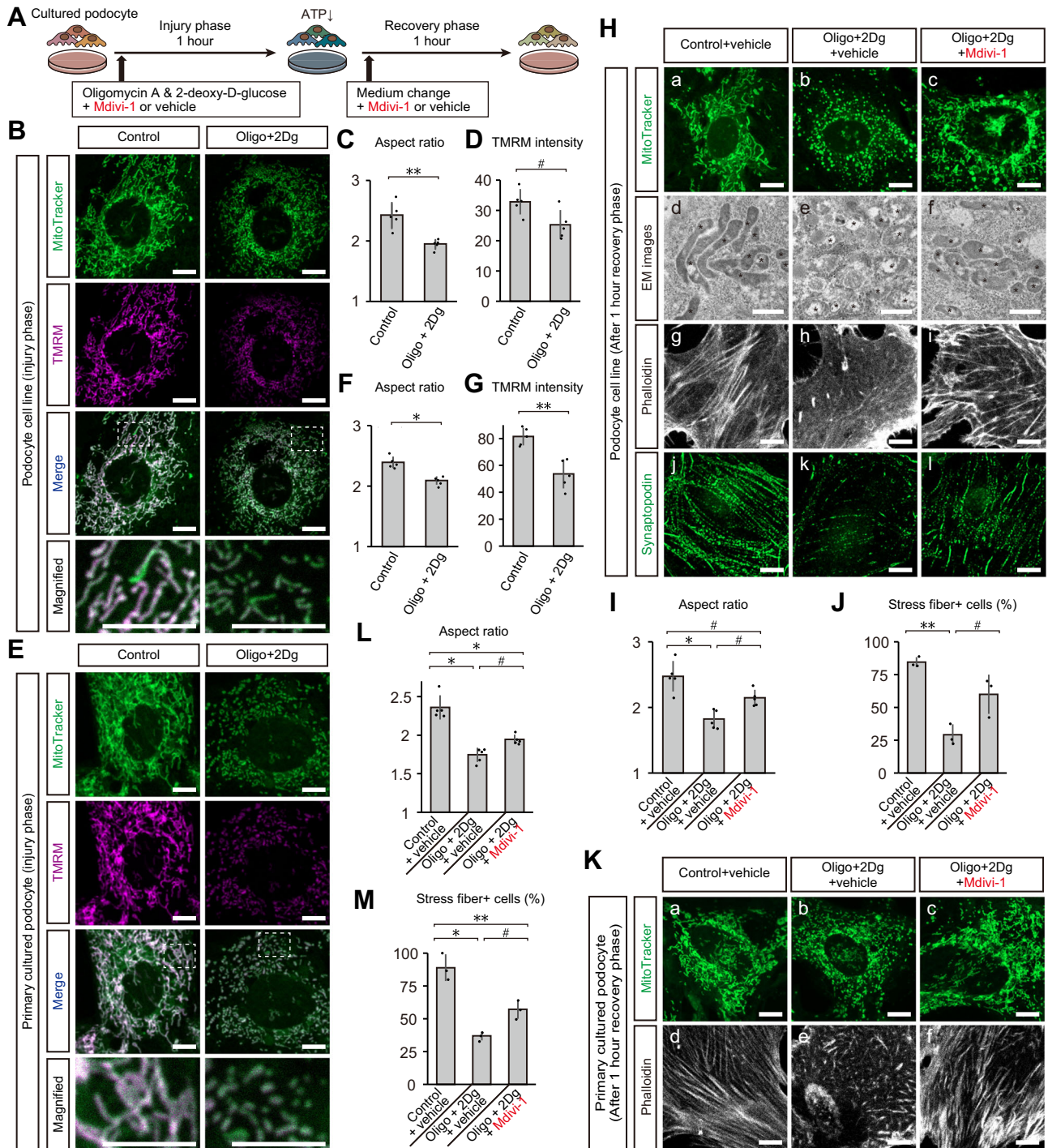


Fig. 8 | Suppression of mitochondrial fission ameliorates podocyte cytoskeletal disarrangement in cultured podocytes. **A** Graphical representation of the experimental design for in vitro IRI. **B** Confocal images of MitoTracker and TMRM staining in podocyte cell line after the injury phase. Bottom panels show magnified images of dashed boxes in merged images. **C** Aspect ratios of mitochondria of podocyte cell line after injury phase. **D** TMRM intensity of mitochondria of podocyte cell line after injury phase. **E** Confocal images of MitoTracker and TMRM staining in primary cultured podocytes after the injury phase. Bottom panels show magnified images of dashed boxes in merged images. **F** Aspect ratios of mitochondria of primary cultured podocytes after injury phase. **G** TMRM intensity of mitochondria of primary cultured podocytes after injury phase. **H** TEM and confocal images of podocyte cell line after the recovery phase: a–c, MitoTracker

staining; d–f, TEM images focusing on mitochondria (asterisks); g–i, actin cytoskeleton visualized by phalloidin labelling; j–l, synaptopodin immunostaining. **I** Aspect ratios of mitochondria of podocyte cell line after recovery phase. **J** Percentages of stress fiber-positive cells in podocyte cell line after the recovery phase. **K** Confocal images of primary cultured podocytes after the recovery phase: a–c, MitoTracker staining; d–f, actin cytoskeleton visualized by phalloidin labelling. **L** Aspect ratios of mitochondria of primary cultured podocytes after recovery phase. **M** Percentages of stress fiber-positive cells in primary cultured podocytes after the recovery phase. Exact *p* values for **(C)**, **(D)**, **(F)**, **(G)**, **(I)**, **(J)**, **(L)**, and **(M)** are shown in Supplementary Table 1, 2. **p* < 0.001; ***p* < 0.01; #*p* < 0.05. Scale bars: 1 μm in d–f for H; 10 μm in **(B)**, **(E)**, a–c and g–l for **(H)**, and **(K)**. EM, electron microscopy; Oligo, oligomycin A; 2-Dg, 2-deoxy-D-glucose; IRI, ischemia reperfusion injury.

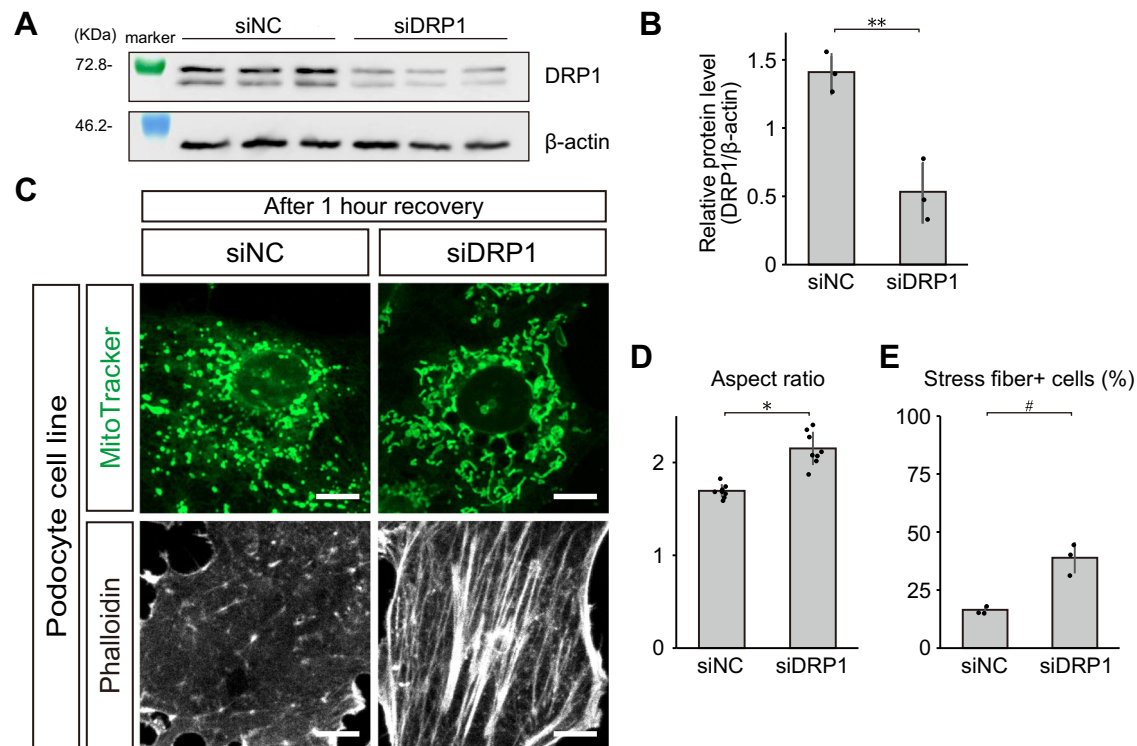


Fig. 9 | DRP1 knockdown ameliorates mitochondrial fragmentation and stress fiber loss in cultured podocytes after ATP depletion stress. A Blotting of DRP1 in cultured podocytes treated with siNC or siDRP1. β-actin was used as a loading control. **B** Relative protein levels of DRP1, standardized by β-actin, in cultured podocytes treated by siNC or siDRP1. Exact *p*-value: ***p* = 0.0077. **C** Confocal images

of MitoTracker and phalloidin staining in podocyte cell line, treated by siNC or siDRP1, after the recovery phase. **D** Aspect ratios of mitochondria of podocyte cell line treated by siNC or siDRP1. Exact *p*-value: **p* = 0.0001. **E** Percentages of stress fiber-positive cells in podocyte cell line treated by siNC or siDRP1. Exact *p*-value: #*p* = 0.0231. **p* < 0.001; ***p* < 0.01; #*p* < 0.05. Scale bars: 20 μm.

during ischemia than collecting ducts, which have robust glycolytic capacity³⁶.

Second, we visualized the dynamic ATP recovery in podocytes after reperfusion. Initial ATP recovery immediately after reperfusion was faster than that of proximal tubules, which have limited ability of glycolysis, suggesting that relatively swift ATP recovery in podocytes might be caused by parallel re-activation of oxidative phosphorylation and anaerobic glycolysis in the beginning of the reperfusion phase. Prolonged ischemia resulted in delayed and insufficient ATP recovery and mitochondrial fragmentation shortly after reperfusion, suggesting that mitochondrial dysfunction could contribute to the ATP shortage, which exceeded the glycolytic reserve for ATP production. Although several reports have suggested that the contribution of mitochondria to energy homeostasis could be less significant in podocytes under physiological conditions because of their high glycolytic capacity^{18,35}, our results suggest that sufficient oxidative phosphorylation is required to maintain podocyte ATP levels, especially under post-ischemic conditions.

We also discovered intraglomerular heterogeneity in ATP dynamics during IRI. Endothelial cells, which have been reported to be largely dependent on glycolytic ATP production³⁷, showed a similar decrease in ATP as podocytes during ischemia, but they exhibited less sufficient recovery after reperfusion than podocytes. Despite insufficient ATP recovery after reperfusion, electron microscopy in the chronic phase of IRI showed only modest pathological changes in endothelial cells. Considering the close interactions between podocytes and endothelial cells^{38–42}, it remains unclear whether ischemia-induced ATP insufficiency in endothelial cells could hamper podocyte-endothelial cross-talk.

Finally, we showed that mitochondrial fragmentation was closely associated with podocyte foot process effacement. Mitochondrial fragmentation was the earliest ultrastructural change in podocytes in

the super-acute phase of IRI (30 min after reperfusion), when foot process effacement was not obvious. Three-dimensional reconstruction effectively showed the disruption of mitochondrial networks and mitochondrial fragmentation shortly after IR. Mitochondrial fragmentation was also observed in the chronic phase of IRI in mice that had undergone prolonged ischemia, and it was associated with foot process effacement of podocytes. Furthermore, ATP recovery in the super-acute phase was inversely correlated with the severity of foot process effacement and mitochondrial fragmentation in the chronic phase. These results are consistent with our previous report, which showed that delayed ATP recovery in the proximal tubules in the super-acute phase predicted interstitial fibrosis in the chronic phase¹⁵. The pathophysiological involvement of mitochondrial fragmentation in foot process effacement was confirmed by the experiments using Mdivi-1, a specific inhibitor of the mitochondrial fission protein DRP1, whereby mitochondrial fragmentation was ameliorated and this restored podocyte structures in cultured podocytes under ATP-depletion stress, slice culture mimicking IRI, and in mice that were subjected to IRI. Taken together, mitochondrial fragmentation and impaired ATP synthesis after ischemia appear to be strongly associated with foot process effacement in the chronic phase of IRI. Nonetheless, we cannot exclude the potential beneficial off-target effects caused by Mdivi-1, as was recently reported by Bordt and colleagues, whereby Mdivi-1 reversibly inhibits mitochondrial complex I and reduces reactive oxygen species production only at higher concentrations⁴³. However, as similar protective effects were also induced by *Drp1* knockdown in cultured podocytes, this suggests that DRP1 and mitochondrial fragmentation in podocytes likely plays pivotal roles in podocyte injury after ischemia. Similar protective effects have also been observed in podocytes deficient for *Drp1* under diabetic stress^{23,25}, though the exact underlying mechanisms remain unclear. Considering that the conditional knockout of *Drp1* alone seems to

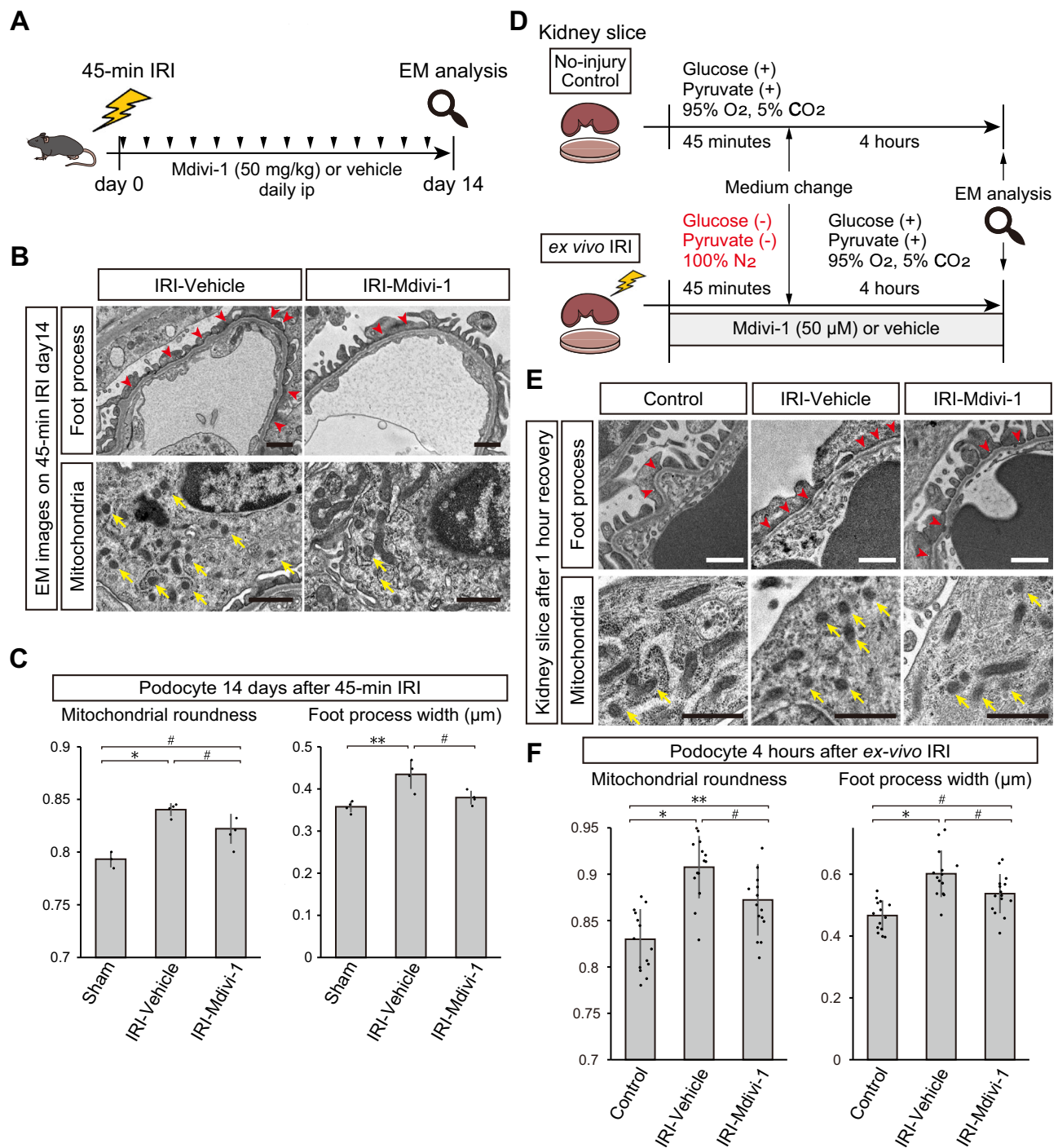


Fig. 10 | Suppression of mitochondrial fission ameliorates podocyte cytoskeleton disarrangement in mice and slice cultured kidney. **A** Graphical representation of the experimental design for **(B and C)**. **B** TEM images of glomerular tufts 14 days after 45-min IRI with Mdivi-1 or vehicle treatment. Upper panels focus on foot processes (red arrows indicating foot process effacement), and lower panels on mitochondria (yellow arrows indicating fragmented mitochondria). **C** Mitochondrial roundness and foot process width of podocytes 14 days after 45-min IRI with Mdivi-1 or vehicle treatment, or sham surgery. Data of sham surgery group in Fig. 6B and C were shown again for comparison. Exact p -value: Sham vs Vehicle: $*p = 0.0006$; Sham vs Mdivi-1: $\#p = 0.0254$; Vehicle vs Mdivi-1: $\#p = 0.0277$ for the left graph and Sham vs Vehicle: $**p = 0.0042$; Vehicle vs Mdivi-1: $\#p = 0.0308$ for the right graph. **D** Graphical representation of the experimental design for

(E and F). **E** TEM images of glomerular tufts after ex vivo IRI with Mdivi-1 or vehicle treatment. Upper panels focus on foot processes (red arrows indicating foot process effacement), and lower panels on mitochondria (yellow arrows indicating fragmented mitochondria). **F** Mitochondrial roundness and foot process width of podocytes after 4-h recovery phase with Mdivi-1 or vehicle treatment or non-injury control. Each dot in the graphs represents the value of each glomerulus. Exact p -value: Control vs Vehicle: $*p < 0.0001$; Control vs Mdivi-1: $**p = 0.0044$; Vehicle vs Mdivi-1: $\#p = 0.0263$ for the left graph and Control vs Vehicle: $*p < 0.0001$; Control vs Mdivi-1: $\#p = 0.0125$; Vehicle vs Mdivi-1: $\#p = 0.0252$ for the right graph. $*p < 0.001$; $**p < 0.01$; $\#p < 0.05$. Scale bars: 1 μm in B and E. EM, electron microscopy; IRI, ischemia reperfusion injury.

show no significant phenotype during a 12-month observation window³⁵, this suggests that the pathophysiological role of DRP1 in podocytes may only become apparent upon stress-induced conditions. Our results indicate that DRP1 may be a potential therapeutic target to prevent podocyte injury after IRI, though further direct validation will be necessary (see below for details).

Ex vivo slice culture is a classic method that can exclude confounding effects such as changes of hydrostatic pressure and neurohormonal mediators, while preserving 3-D tissue organization⁴⁴. Although increased hydrostatic pressure has been suggested as one of the causes of secondary glomerular injury after tubular injury⁴⁵, our ex vivo model has the advantage of being able to exclude this, suggesting that IRI could directly induce chronic podocyte injury through ATP depletion and mitochondrial fragmentation.

Because the degree of proteinuria in our model was moderate, we cannot exclude the contribution of decreased protein absorption in injured tubules. However, given that our data also directly demonstrated podocyte injury, and given that clinical evidence shows proteinuria and glomerulosclerosis after AKI and kidney transplantation^{5,7,12,46–49}, it is highly likely that changes in podocyte ATP levels during ischemia reperfusion is strongly linked to podocyte injury in the chronic phase.

A remaining question is how mitochondrial fragmentation induces foot process effacement in ischemic injury. We did not observe significant podocyte loss despite the signs of severe mitochondrial fragmentation, a well-known trigger of cell death⁵⁰. However, podocyte injury that we observed on day 14 of IRI could progress over time. A previous study showed that glomerulosclerosis, a consequence of significant podocyte loss, increases 8 months after IRI in rats, compared to 1 month after IRI, and is significantly reduced by SS-31 treatment, which enhances mitochondrial ATP production in podocytes⁵¹. Therefore, it remains unclear how mitochondrial dysfunction after ischemic injury influences the long-term viability of podocytes. Fragmented mitochondria are suggested to have reduced capacity for ATP production⁵², and a stable ATP supply is considered essential for maintaining podocyte foot processes. In cultured Purkinje cells, the disruption of mitochondrial trafficking into dendrites was shown to perturb actin dynamics likely via an energy shortage, resulting in malformation of dendrites⁵³. Podocytes and neurons are highly differentiated cells possessing complicated cytoplasmic processes and express common tissue-specific proteins, including synaptopodin and nephrin⁵⁴. Considering these similarities, disruption of mitochondrial network and reduction in ATP in podocyte foot processes after ischemia reperfusion could hamper the actin dynamics and lead to morphological abnormality of foot processes effacement as shown in Purkinje cells.

The extent to which ischemic podocyte injury affects long term renal prognosis is unknown; however, mitochondrial fragmentation and foot process effacement in podocytes in the chronic phase may have an impact on renal prognosis. Previous clinical studies showed that persistent proteinuria is a risk factor for kidney disease progression after kidney transplantation or AKI^{7,48}. In the current study, albuminuria in the chronic phase after IRI increased with ischemia time prolonged (i.e. severity of injury). Thus, glomerular injury after IRI could be an important prognostic factor.

Our study has several technical limitations. Firstly, deep glomeruli in long-loop nephrons cannot be observed by our method. However, a paper analyzing nephrectomized samples showed that age-related glomerulosclerosis, which may be related to ischemia caused by arteriosclerosis, are more pronounced in surface glomeruli than in deep glomeruli⁵⁵, suggesting that the observations from the kidney surface may provide useful information. Secondly, although GO-ATeam2 biosensor is less susceptible to pH change than other ATP probes¹⁴, there is a possibility that the extent of ATP decrease in podocytes after IRI may be underestimated due to intracellular

acidosis, which was observed in cultured podocytes under stress conditions⁵⁶. Intracellular acidosis could increase the OFF-to-GFP ratio¹⁴, thus, ATP decline in podocytes could be even more dynamic than we observed. Thirdly, our ATP imaging method cannot distinguish between ATP production and consumption. Although the insufficient ATP recovery after ischemia reperfusion is most likely due to impaired oxidative phosphorylation, we cannot rule out the possibility of increased ATP consumption. Finally, to conclusively determine the role of DRP1 in podocyte injury after IRI, our findings need to be further validated using *Drp1* conditional knockout mice, which warrants future investigation.

In sum, our findings showing that ATP depletion and mitochondrial injury in podocytes might contribute to podocyte injury in the chronic phase of IRI provides several insights and potential treatment options for IRI and its transition to chronic disease.

Methods

Ethical statement

All animal studies were approved by the Animal Research Committee, Graduate School of Medicine, Kyoto University (No. MedKyo22183), and were performed in accordance with the National Institute of Health Guide for the Care and Use of Laboratory Animals.

Mice

GO-ATeam2 and GO-ATeam2 flox/+ mice were generated in our laboratory and are described in separate papers^{13,16}. *Nphs1*-Cre mice were generated as previously described⁵⁷. *Tie2*-Cre mice were purchased from The Jackson Laboratory (Bar Harbor, ME, USA)⁵⁸. Female C57BL/6J mice were purchased from SLC (Shizuoka, Japan). Female mice between 9 and 13 weeks of age, which were housed in a specific pathogen-free facility at 50 ± 10 % humidity and 24 ± 2 °C under 14 h/10 h light and dark cycle with access to water and regular diet ad libitum, were used for the experiments.

Mouse treatment

Mice were anaesthetized using isoflurane inhalation (induction: 2–3%; maintenance: 1.5%). The left kidney was exteriorized through a small incision. Kidney ischemia was induced by clamping the left renal pedicle by a microclip for each length of time⁵⁹. The core body temperature and kidney surface temperature were maintained at 36.5 °C during ischemia and reperfusion. The heart rate and breathing rate were maintained at over 450 bpm and over 100 breaths per minute, respectively. Mdivi-1, a GTPase inhibitor that specifically inhibits DRP1, was chosen for pharmacological suppression of mitochondrial fission. Mdivi-1 (50 mg/kg, Selleck Chemicals, Houston, TX, USA) or vehicle (DMSO) was administered intraperitoneally 30 min after reperfusion and then daily for 14 days before euthanasia for analysis ($n = 4$ mice per group; Fig. 10A–C). Regimen of Mdivi-1 treatment was determined based on previous studies and the estimated half-life (12 h)^{24,25,60}.

Cell culture and treatment

A conditionally immortalized mouse podocyte cell line was kindly provided by Professor Peter Mundel (Harvard Medical School, Boston, MA, USA). The cells were maintained in RPMI 1640 medium containing 10% heat-inactivated fetal bovine serum, 1 mM sodium pyruvate, and 0.01 mM HEPES in a 5% CO₂ atmosphere. To sustain proliferation, murine interferon (INF)- γ (10 U/mL; R&D Systems, Minneapolis, MN, USA) was added to the medium, and the cells were maintained at 33 °C. To induce differentiation, cells were seeded in a dish coated with rat collagen type 1 (0.12 mg/mL; Corning, NY, USA) and maintained in medium without INF- γ at 37 °C for 10 days before the experiments. For podocyte primary culture, kidneys were harvested from 8–12-week-old wild-type mice after perfusion of 20 ml PBS containing 1% Dynabeads M450 tosylactivated (Invitrogen, Waltham, MA, USA) under anesthesia using isoflurane inhalation.

Kidney samples were roughly minced and processed under two cycles of incubation (37 °C, 15 min) and dissociation using gentle-MACS Dissociator (Miltenyi Biotech, Bergisch Gladbach, Germany) in RPMI1640 medium containing 0.01 mM HEPES and Liberase TH (0.25 mg/ml; Roche, Mannheim, Germany) and Dnase I (1 mg/ml; Roche) before purification by a magnet stand and dissociation tubes. Purified glomeruli were seeded in collagen-coated dishes and maintained in RPMI 1640 medium containing 10% heat-inactivated fetal bovine serum at 37 °C for 5 days before the out-growth, which consists mostly of podocytes, were collected and filtered through 40 µm mesh. Collected podocytes were maintained in RPMI 1640 medium containing 10% heat-inactivated fetal bovine serum at 37 °C for 4 weeks for induction of differentiation before experiments^{61,62}. To assess the effect of ATP depletion on the podocyte cytoskeleton, oligomycin A (10 µM; LKT Laboratories, St. Paul, MN, USA) and 2-deoxy-D-glucose (20 mM; FUJIFILM Wako Chemicals, Osaka, Japan) or vehicle (DMSO and PBS) were added to the medium, and cells were incubated for 1 h at 37 °C in 5% CO₂ (injury phase). We used Oligomycin A and 2-deoxy-D-glucose to inhibit ATP production. Oligomycin A directly inhibits ATP synthase, and 2-deoxy-D-glucose inhibits the glycolytic pathway because its metabolite is not a substrate for glucose-6-phosphate dehydrogenase or phosphohexose isomerase. Dosing of oligomycin A and 2-deoxy-D-glucose were determined based on reported IC50 (oligomycin A: 0.21–3.8 µM⁶³; 2-deoxy-D-glucose: 1–10 mM⁶⁴) and other previous studies^{18,35}. After injury phase, the dishes were thoroughly washed with PBS, and cells were incubated in fresh medium for 1 h at 37 °C in 5% CO₂ (recovery phase). To assess the protective effect of inhibiting mitochondrial fission in podocytes, Mdivi-1 (50 µM; Selleck Chemicals) or vehicle (DMSO) was added to the medium in both the injury and recovery phases. Dosing of Mdivi-1 supplementation for in vitro and ex vivo experiments was determined based on IC50 indicated on its datasheet (1–10 µM, Selleck Chemicals) and a pilot study. To assess the mitochondrial membrane potential and morphology, TMRM (100 nM; Thermo Fisher Scientific, Waltham, MA, USA) and MitoTracker Green (200 nM; Thermo Fisher Scientific) were added to the medium 30 min before observation. Mitochondrial membrane potential and aspect ratio of mitochondria were assessed with ImageJ (National Institutes of Health, Bethesda, MD, USA). To determine TMRM intensity and aspect ratio of mitochondria, five cells per group were assessed in Fig. 8C, D, F, G, I, and L, and eight cells per group were assessed in Fig. 9D. Values of each cell are indicated by dots in Fig. 8C, D, F, G, I, L, and Fig. 9D.

Knockdown by siRNA

Nontargeting control oligonucleotide (D-001810-10-05) and siRNA against mouse *Drp1* (L-054815-01-005) were purchased from Horizon Discovery (Cambridge, UK). Transfection of siRNA oligonucleotide was performed using DharmaFECT-2 siRNA transfection reagent (Horizon Discovery) per manufacturer's instructions on day 8 of differentiation which is 48 h before experiments.

Estimation of intracellular ATP concentrations

Murine embryonic fibroblasts (MEFs) were freshly isolated from GO-ATeam2 mouse embryos at E13.5 and were maintained in DMEM high glucose medium containing 10% heat-inactivated fetal bovine serum at 37 °C for 5 days for expansion before experiments. For estimation of intracellular ATP concentration, MEFs that were treated by Seahorse XF Plasma membrane permeabilizer (1 nM; Agilent Technologies, Santa Clara, CA, USA) for 10 min were observed in calculation buffer containing arbitrary concentrations of ATP (Thermo Fisher Scientific). The plot was fitted with a

regression equation.

$$[\text{ATP}] \text{ mM} = \frac{\text{ATP ratio} - 0.553}{0.449} \quad (1)$$

Urinary albumin-to-creatinine ratio measurement

The urinary albumin-to-creatinine ratios were compared between mice that received sham procedures and 45-min IRI ($n = 5$ mice per group, one mouse excluded due to failed procedure of ischemia reperfusion from day 14–15 data). To avoid contamination of urine produced by the contralateral kidney, the contralateral ureter was ligated under anesthesia. Ligation of the contralateral ureters was performed under inhalation anesthesia 6 days, 13 days, or 27 days after IRI or sham surgery. To minimize the influence of post-surgical inflammation and dehydration, 24 h of recovery phase was set before 24-h urine collection (Fig. 1G). The urinary albumin concentrations were determined by ELISA kit (Albuwell M, Ethos Biosciences, Logan Township, NJ, USA), and urinary creatinine levels were determined by Jaffe's method (LabAssay creatinine, FUJIFILM Wako Chemicals, Osaka, Japan). Urinary albumin concentrations were normalized to urinary creatinine concentrations.

Microscopy

For multiphoton microscopy, we used an FV1200MPE-BX61W1 upright microscope equipped with a 25×/1.05NA water-immersion objective lens (XLPLN25XW-MP; Olympus, Tokyo, Japan), an Insight DeepSee Ultrafast Laser (Spectra Physics, Mountain View, CA, USA), an IR-cut filter, BA750RXD, two dichroic mirrors, DM505 and DM690, and two emission filters, BA495-540 (Olympus) for green fluorescent protein (GFP) and BA562-596 (Olympus) for kusabira orange fluorescent protein (OFP), with the excitation wavelength of 930 nm. Immunofluorescence staining was analyzed using confocal microscopes (FV1000D; Olympus and LSM900; ZEISS, Jena, Germany).

In vivo multiphoton imaging

After anesthetization and flank incision, the mouse kidney was attached to a vacuum-stabilized cup⁶⁵. The core body temperature and kidney surface temperature were controlled using a heating system. We took images 16 µm and 40 µm from the kidney surface to assess ATP in tubules and glomeruli, respectively. Distal tubules and collecting ducts were identified according to the criteria in our previous work¹⁴. Briefly, we identified these segments by co-staining of the GO-ATeam2 biosensor and cell type markers as well as by live imaging after injection of fluorescence-labelled dextran¹⁵. Images were analyzed using MetaMorph software (Universal Imaging, West Chester, PA, USA).

Analysis of OFP/GFP ratio changes

Quantification of the OFP/GFP ratio (ATP^{ratio}) was performed using MetaMorph software. The ATP^{ratio} in podocytes was determined by dividing the mean fluorescent intensity (MFI) of OFP in each podocyte by that of GFP (Supplementary Fig. 2A). The ATP^{ratio} in tubular sections was calculated by dividing the MFI of OFP in each continuous tubule by that of GFP¹⁵. Averages of the ATP^{ratio} in at least four podocytes were used as the mean podocyte ratio in each glomerulus in healthy non-treated kidneys. To analyze the inter-glomerular variation of ATP^{ratio} of podocytes under the normal condition, the mean podocyte ATP^{ratio} in each glomerulus was determined in 49 glomeruli from five mice and was indicated as a dot in Fig. 2E. The tubular ATP^{ratios} in normal condition were measured in 20 proximal tubules, 17 distal tubules, and 10 collecting ducts from 4 mice and were indicated as dots in Fig. 2E. In time-lapse imaging of the kidneys, the average ATP^{ratio} in at least four

cells in one glomerulus for each time point was used as the ATP^{ratio} for each mouse, and the mean ATP^{ratio} in each group is shown as a dot at each timepoint ($n = 4$ mice per group; Figs. 3C, 4B, *Nphs1*-ATeam and *Tie2*-ATeam in Fig. 5, E and G, and Supplementary Fig. 3, $n = 8$ mice per group; Fig. 5B and 'Cells with slow ATP decline' in Fig. 5E). For tubular ATP, the average ATP^{ratio} from five proximal tubules (S1 segment), two to six distal tubules, and two to three collecting ducts in one image for each time point were used as the ATP^{ratio} for each mouse ($n = 4$ mice; Fig. 3E). The mean ATP^{ratio} in each group was shown as a dot in each timepoint (Fig. 3C, E, Figs. 4B, 5B, E, G). ATP % recovery after 30 min of reperfusion was determined as shown below.

$$\text{ATP\% recovery} = \frac{\text{ATP}^{\text{ratio}} \text{ after 30 - min reperfusion} - \text{bottom ATP}^{\text{ratio}}}{\text{ATP}^{\text{ratio}} \text{ before ischemia} - \text{bottom ATP}^{\text{ratio}}} \times 100 \quad (2)$$

Data from Figs. 4B, 5G were used to determine ATP % recovery in Figs. 4D, 5H, respectively ($n = 4$ mice per group).

The change of ATP^{ratio} after one minute of reperfusion ($\Delta\text{ATP}^{\text{ratio}}$) was determined using the equation below.

$$\Delta\text{ATP}^{\text{ratio}} = \text{ATP}^{\text{ratio}} \text{ after 1 min reperfusion} - \text{ATP}^{\text{ratio}} \text{ before reperfusion} \quad (3)$$

To determine $\Delta\text{ATP}^{\text{ratio}}$, data from Fig. 4B were used ($n = 4$ mice per group; Fig. 4C).

Immunohistochemistry

Harvested kidney samples were fixed in 4% paraformaldehyde, incubated in 20% sucrose in PBS at 4 °C overnight and incubated in 30% sucrose at 4 °C overnight. OCT-embedded kidneys were cryo-sectioned into 6.0 μm sections. The following primary antibodies were used for immunostaining: anti-nephrin (R&D Systems, Minneapolis, MN, USA), anti-WT1 (abcam, Cambridge, UK), anti-GFP (abcam), anti-nestin (Immuno-Biological Laboratories, Gunma, Japan), anti-CD31 (BD, Franklin lakes, NJ, USA), anti-podocin (Sigma-Aldrich, St. Louis, MO, USA), anti-megalin (Santa Cruz Biotechnology, Dallas, TX, USA), and anti-DRP1 (abcam) antibodies. WT1-positive cells were manually analyzed in 20 glomeruli for each mouse. Mean fluorescence intensity of podocyte markers was assessed with MetaMorph software. Samples for the analysis of WT1 positive cells and podocyte marker expression (Fig. 1D–F) were obtained from the same mice that were used for Fig. 1A–C (45-min IRI: 4 mice; sham: 4 mice).

Immunocytochemistry

After 10 min of fixation in 4% paraformaldehyde, the cells were stained with anti-synaptopodin antibody (PROGEN, Heidelberg, Germany), and Alexa 647-conjugated phalloidin (Thermo Fisher Scientific, Waltham, MA, USA). Stress fiber quantification was performed manually in each individual cell in independent images, where a stress fiber was defined as a phalloidin-positive structure spanning the length of the cell. Broken or arc-shaped structures were not counted as a stress fiber⁶⁶. Three dishes per group were assessed to compare percentages of stress fiber positive cells. In each dish, eight confocal images were obtained, and all cells in the images (at least 30 cells per dish) were assessed to determine the percentages of stress fiber positive cells.

Periodic acid-Schiff (PAS) staining

Kidney samples were fixed in Carnoy solution, embedded in paraffin, sectioned into 2.0 μm sections, and stained with PAS. All of PAS-stained samples were analyzed with BZ-X710 microscope (Keyence, Osaka, Japan) using BZ-X Viewer 01.03.00.05 software (Keyence).

Electron microscopy

The samples were fixed in 2% glutaraldehyde/4% paraformaldehyde. The ultrathin sections were stained with lead citrate and uranyl

acetate. Images at $\times 3000$ and $\times 5000$ magnitude were obtained using a H7650 transmission electron microscope (Hitachi High-tech, Tokyo, Japan). Quantification of morphological changes in the foot processes and mitochondria was assessed using MetaMorph software. Foot process widths (FPW) were determined using the equation below^{67,68}.

$$\text{FPW} = \frac{\pi}{4} \times \frac{\sum \text{GBM length}}{\sum \text{slits}} \quad (4)$$

$\Sigma\text{GBM length}$ and Σslits indicate the total glomerular basement membrane measured and the total number of slits counted in one glomerulus.

The average foot process width from at least five glomeruli was used to determine the foot process width of each mouse. The average foot process width in each mouse is indicated as a dot in Figs. 1B, J, 6B, 7B, E, F, 10C. Determining the average foot process widths included 14 wild type mice (30-min IRI: 6 mice; 45-min IRI: 4 mice; sham: 4 mice) in Fig. 1A–C, 10 wild type mice (5 mice per group) in Fig. 1J, 6 wild type mice (3 mice per group) in Fig. 6B, 20 GO-ATeam2 mice (4 mice per group) in Fig. 7A, B, E, F, 8 wild type mice (4 mice per group with 3 sham-treated mice from Fig. 6A, B) in Fig. 10B, C. Mitochondrial roundness (MR) was determined using the equation below⁶⁹.

$$\text{MR} = 4\pi \times \frac{S}{L^2} \quad (5)$$

S and L indicate surface area and perimeter of mitochondria, respectively.

For in vivo analysis, the mean mitochondrial roundness in at least 15 images (three images in each glomerulus, and at least five glomeruli in each mouse) were averaged to determine the mean value for each mouse. Determining the mean mitochondrial roundness included 15 wild type mice (3 mice per group) in Fig. 6C, 20 GO-ATeam2 mice (4 mice per group) in Fig. 7C, and 8 wild type mice (4 mice per group with 3 sham-treated mice from Fig. 6C) in Fig. 10B, C.

To determine the average foot process widths and mitochondrial roundness in slice cultured kidneys (mean values in each glomerulus), 3 slices per group were assessed by electron microscopy, and all of assessable glomeruli in obtained images were included in analysis. Foot process widths and mitochondrial roundness from three slices of each group were compared collectively between three experimental groups (control vs vehicle-treated IRI vs Mdivi-1-treated IRI).

In Figs. 1C, 10F, values of foot process width or mitochondrial roundness in each glomerulus are indicated as dots (numbers of glomeruli; sham: 38; 30-min IRI: 62; 45-min IRI: 40 in Fig. 1C; control: 14; IRI-vehicle: 14; IRI-Mdivi-1: 15 in Fig. 10F). For focused-ion beam/scanning electron microscopy (FIB/SEM), kidney tissues, which were harvested 30 min after sham surgery or 45-min IRI, were fixed and embedded in epoxy resin, and serial FIB/SEM images were obtained at 50-nm increments using a Crossbeam540 (Carl Zeiss, Stuttgart, Germany)⁷⁰. Three female wild-type mice from each group were used for the analysis. One podocyte that was applicable to the whole-cell analysis was chosen for each serial image. Mitochondria and nucleus segmentation was performed using the Microscopy Image Browser⁷¹, and a three-dimensional image was reconstituted using Imaris software (Oxford Instruments, Oxford, UK) for each mouse.

Ex vivo IRI model

We established an ex vivo IRI model²⁰. After adequate anesthesia using isoflurane, kidneys of 10-week-old male wild-type mice were harvested and decapsulated. They were immediately sliced at 300 μm with a vibratome (VT1000S; Leica Microsystems, Wetzlar, Germany) in ice-cold buffer that was with 95% O₂ and 5% CO₂ and contained 97.5 mM NaCl, 5 mM KCl, 0.24 mM NaH₂PO₄, 0.96 mM Na₂HPO₄, 10 mM CH₃COONa, 25 mM NaHCO₃, 10 mM glucose, 5 mM Na pyruvate,

0.6 mM MgSO₄, and 1 mM CaCl₂, as previously reported with a few modifications⁷². To induce ischemia-like conditions, the normal buffer was replaced by the ischemia buffer, which contained no energy sources and was saturated with nitrogen, as previously reported in the heart and cell culture^{73,74}. To induce reperfusion-like conditions, ischemia buffer was replaced by normal buffer, and oxygenation was resumed. To assess the protective effect of inhibiting mitochondrial fission in podocytes, Mdivi-1 (50 μM; Selleck Chemicals) or vehicle (DMSO) was added to the medium in both the injury and recovery phases. Non-injury control was maintained in the same conditions to the injury groups except energy deprivation and drug supplementation.

Western blot analysis

Cell lysates were prepared from cultured podocytes by sonicating in RIPA lysis buffer containing 1% phosphatase inhibitor cocktail 2 (Sigma-Aldrich), 1% phosphatase inhibitor cocktail 3 (Sigma-Aldrich), and 1% Halt protease inhibitor cocktail (Thermo Fisher Scientific). Homogenates were centrifuged (15,000 rpm, 20 min, 4 °C) and the protein concentration of the supernatant was measured by using the TaKaRa BCA protein assay kit (Takara Bio, Kusatsu, Japan). Equal volumes of remaining cell lysate supernatants were boiled with β-mercaptoethanol (95 °C, 5 min). Proteins were separated using 9% SDS-PAGE and transferred to a nitrocellulose membrane (Bio-Rad Laboratories, Hercules, CA, USA). The membranes were blocked with 5% skim milk/PBST for 1 h at room temperature and incubated with primary antibody diluted in 5% skim milk/PBST at 4 °C overnight. The membranes were washed in PBST and were incubated with the relevant secondary antibody (1:3000) for 1 h at room temperature. After thoroughly washed, the bands were detected using Amersham ECL Prime Chemiluminescent Western blotting kit (Cytiva, Amersham, UK) with ImageQuant LAS 500 (Cytiva). Protein expression was assessed with ImageJ software (National Institutes of Health, Bethesda, MD, USA) and was compared between siDRP1 podocytes and siNC podocytes (3 dishes per group)⁷⁵. The following primary antibodies were used: rabbit anti-DRP1 antibody (1:1000; ab184274, abcam, Cambridge, UK) and rabbit anti-β-actin antibody (1:1000; CST4967, Cell Signaling Technology, Danvers, MA, USA).

Statistics and reproducibility

Results are presented as mean ± standard deviation (SD). Statistical analysis was performed using JMP Pro ver.15.2.0 (SAS Institute, Cary, NC, USA) and EZR ver.1.55⁷⁶. A two tailed Student's *t*-test was used for a comparison between two groups (Figs. 1E, F, H, J, 5H, 6B, 8C, D, F, G, 9B, D, E). Comparisons between more than three groups were assessed using analysis of variance (ANOVA) with a Tukey–Kramer *post hoc* test (Figs. 1B, 4D, 6C, 7B, C, 8I, J, L, M, 10C, F). Correlations were determined using Pearson's correlation analysis (Fig. 7E, F and Supplementary Fig. 2C). Trend analysis was performed using the two-sided Jonckheere–Terpstra test (Figs. 4C, D, 6C, 7B–D). Statistical significance was defined as *p* < 0.05. Data are represented as means ± standard deviation (Figs. 1B, E, F, H, J, 3C, E, 4D, 5, B, E, G, H, 6B, C, 7B–D, 8C, D, F, G, I, J, L, M, 9B, D, E, 10C, F, and Supplementary Fig. 3). Exact *p* values in Fig. 8 are shown in Supplementary Tables 1, 2, and exact *p* values in other Figures are shown in legends.

ATP images of glomeruli and tubules before and after ischemia and findings on ATP dynamics that are mentioned in our study (Figs. 2A–C, 3A, B, D, 4A, 5A, C, D, F, and Supplementary Fig. 5), and morphological and pathological analysis in glomerulus after ischemia that are mentioned in our study (Figs. 1A, D, I, 2D, 6A, 7A, Supplementary Figs. 1, 4A–D, 6A, B, 7A, B) were reproduced repeatedly in our experiments. Pathological changes after ATP depletion in cultured podocytes were consistent in three biological replicates (Figs. 8, 9C, D, E).

Reporting summary

Further information on research design is available in the Nature Portfolio Reporting Summary linked to this article.

Data availability

All data supporting the findings of this study are provided in Supplementary Information and Source Data file. Source Data file is provided with this paper. Source data are provided with this paper.

References

- Kaufman, J., Dhakal, M., Patel, B. & Hamburger, R. Community-acquired acute renal failure. *Am. J. Kidney Dis.* **17**, 191–198 (1991).
- Mehta, R. L. et al. Spectrum of acute renal failure in the intensive care unit: the PICARD experience. *Kidney Int* **66**, 1613–1621 (2004).
- Lewington, A. J., Cerdá, J. & Mehta, R. L. Raising awareness of acute kidney injury: a global perspective of a silent killer. *Kidney Int* **84**, 457–467 (2013).
- Chertow, G. M., Burdick, E., Honour, M., Bonventre, J. V. & Bates, D. W. Acute kidney injury, mortality, length of stay, and costs in hospitalized patients. *J. Am. Soc. Nephrol.* **16**, 3365–3370 (2005).
- Parr, S. K. et al. Acute kidney injury is a risk factor for subsequent proteinuria. *Kidney Int* **93**, 460–469 (2018).
- Horne, K. L., Packington, R., Monaghan, J., Reilly, T. & Selby, N. M. Three-year outcomes after acute kidney injury: results of a prospective parallel group cohort study. *BMJ Open* **7**, e015316 (2017).
- Hsu, C. Y. et al. Post-acute kidney injury proteinuria and subsequent kidney disease progression: the assessment, serial evaluation, and subsequent sequelae in acute kidney injury (ASSESS-AKI) study. *JAMA Intern Med* **180**, 402–410 (2020).
- Faul, C., Asanuma, K., Yanagida-Asanuma, E., Kim, K. & Mundel, P. Actin up: regulation of podocyte structure and function by components of the actin cytoskeleton. *Trends Cell Biol.* **17**, 428–437 (2007).
- Gujarati, N. A., Vasquez, J. M., Bogenhagen, D. F. & Mallipattu, S. K. The complicated role of mitochondria in the podocyte. *Am. J. Physiol. Ren. Physiol.* **319**, F955–F965 (2020).
- Yuan, Q. et al. Role of pyruvate kinase M2-mediated metabolic reprogramming during podocyte differentiation. *Cell Death Dis.* **11**, 355 (2020).
- Akchurin, O. & Reidy, K. J. Genetic causes of proteinuria and nephrotic syndrome: impact on podocyte pathobiology. *Pediatr. Nephrol.* **30**, 221–233 (2015).
- Denic, A. et al. Changes in glomerular volume, sclerosis, and ischemia at 5 years after kidney transplantation: incidence and correlation with late graft failure. *J. Am. Soc. Nephrol.* **34**, 346–358 (2023).
- Koitaishi, N. et al. Visualizing ATP dynamics in live mice. Preprint at *BioRxiv* <https://doi.org/10.1101/2020.06.10.143560> (2020).
- Nakano, M., Imamura, H., Nagai, T. & Noji, H. Ca²⁺ regulation of mitochondrial ATP synthesis visualized at the single cell level. *ACS Chem. Biol.* **6**, 709–715 (2011).
- Yamamoto, S. et al. Spatiotemporal ATP dynamics during AKI predict renal prognosis. *J. Am. Soc. Nephrol.* **31**, 2855–2869 (2020).
- Yamamoto, M., Kim, M., Imai, H., Itakura, Y. & Ohtsuki, G. Microglia-triggered plasticity of intrinsic excitability modulates psychomotor behaviors in acute cerebellar inflammation. *Cell Rep.* **28**, 2923–2938.e2928 (2019).
- Kawamoto, S. et al. A novel reporter mouse strain that expresses enhanced green fluorescent protein upon Cre-mediated recombination. *FEBS Lett.* **470**, 263–268 (2000).
- Ozawa, S. et al. Glycolysis, but not mitochondria, responsible for intracellular ATP distribution in cortical area of podocytes. *Sci. Rep.* **5**, 18575 (2015).
- Hagmann, H. & Brinkkoetter, P. T. Experimental models to study podocyte biology: stock-taking the toolbox of glomerular research. *Front Pediatr.* **6**, 193 (2018).
- Yamamoto, S. et al. Visualization of intracellular ATP dynamics in different nephron segments under pathophysiological conditions

- using the kidney slice culture system. *Kidney Int* **106**, 470–481 (2024).
21. Ralto, K. M. & Parikh, S. M. Mitochondria in acute kidney injury. *Semin Nephrol.* **36**, 8–16 (2016).
 22. Hall, A. M., Rhodes, G. J., Sandoval, R. M., Corridon, P. R. & Molitoris, B. A. In vivo multiphoton imaging of mitochondrial structure and function during acute kidney injury. *Kidney Int* **83**, 72–83 (2013).
 23. Wang, W. et al. Mitochondrial fission triggered by hyperglycemia is mediated by ROCK1 activation in podocytes and endothelial cells. *Cell Metab.* **15**, 186–200 (2012).
 24. Yuan, Y. et al. p53/Drp1-dependent mitochondrial fission mediates aldosterone-induced podocyte injury and mitochondrial dysfunction. *Am. J. Physiol. Ren. Physiol.* **314**, F798–F808 (2018).
 25. Ayanga, B. A. et al. Dynamin-related protein 1 deficiency improves mitochondrial fitness and protects against progression of diabetic nephropathy. *J. Am. Soc. Nephrol.* **27**, 2733–2747 (2016).
 26. Imasawa, T. & Rossignol, R. Podocyte energy metabolism and glomerular diseases. *Int J. Biochem Cell Biol.* **45**, 2109–2118 (2013).
 27. Gyarmati, G. et al. Advances in renal cell imaging. *Semin Nephrol.* **38**, 52–62 (2018).
 28. Ashworth, S. L., Sandoval, R. M., Tanner, G. A. & Molitoris, B. A. Two-photon microscopy: visualization of kidney dynamics. *Kidney Int* **72**, 416–421 (2007).
 29. Peti-Peterdi, J., Kidokoro, K. & Riquier-Brison, A. Novel in vivo techniques to visualize kidney anatomy and function. *Kidney Int* **88**, 44–51 (2015).
 30. Scott, I. D. & Nicholls, D. G. Energy transduction in intact synaptosomes. Influence of plasma-membrane depolarization on the respiration and membrane potential of internal mitochondria determined in situ. *Biochem J.* **186**, 21–33 (1980).
 31. Snyder, J. W., Pastorino, J. G., Thomas, A. P., Hoek, J. B. & Farber, J. L. ATP synthase activity is required for fructose to protect cultured hepatocytes from the toxicity of cyanide. *Am. J. Physiol.* **264**, C709–C714 (1993).
 32. Di Lisa, F. et al. Mitochondrial membrane potential in single living adult rat cardiac myocytes exposed to anoxia or metabolic inhibition. *J. Physiol.* **486**, 1–13 (1995).
 33. Guder, W. G. & Ross, B. D. Enzyme distribution along the nephron. *Kidney Int* **26**, 101–111 (1984).
 34. Lee, J. W., Chou, C. L. & Knepper, M. A. Deep sequencing in microdissected renal tubules identifies nephron segment-specific transcriptomes. *J. Am. Soc. Nephrol.* **26**, 2669–2677 (2015).
 35. Brinkkoetter, P. T. et al. Anaerobic glycolysis maintains the glomerular filtration barrier independent of mitochondrial metabolism and dynamics. *Cell Rep.* **27**, 1551–1566.e1555 (2019).
 36. Bagnasco, S., Good, D., Balaban, R. & Burg, M. Lactate production in isolated segments of the rat nephron. *Am. J. Physiol.* **248**, F522–F526 (1985).
 37. Du, W., Ren L., Hamblin M. H. & Fan Y. Endothelial Cell Glucose Metabolism and Angiogenesis. *Biomedicines* **9**, 147 (2021).
 38. Siddiqi, F. S. & Advani, A. Endothelial-podocyte crosstalk: the missing link between endothelial dysfunction and albuminuria in diabetes. *Diabetes* **62**, 3647–3655 (2013).
 39. Eremina, V. et al. VEGF inhibition and renal thrombotic microangiopathy. *N. Engl. J. Med.* **358**, 1129–1136 (2008).
 40. Qi, H. et al. Glomerular endothelial mitochondrial dysfunction is essential and characteristic of diabetic kidney disease susceptibility. *Diabetes* **66**, 763–778 (2017).
 41. Ueda, S. et al. ENOS deficiency causes podocyte injury with mitochondrial abnormality. *Free Radic. Biol. Med.* **87**, 181–192 (2015).
 42. Daehn, I. et al. Endothelial mitochondrial oxidative stress determines podocyte depletion in segmental glomerulosclerosis. *J. Clin. Invest* **124**, 1608–1621 (2014).
 43. Bordt, E. A. et al. The putative Drp1 inhibitor mdivi-1 is a reversible mitochondrial complex I inhibitor that modulates reactive oxygen species. *Dev. Cell* **40**, 583–594.e586 (2017).
 44. Saitta, B. et al. Ex vivo kidney slice preparations as a model system to study signaling cascades in kidney epithelial cells. *Methods Cell Biol.* **153**, 185–203 (2019).
 45. Chihanga, T. et al. NMR spectroscopy and electron microscopy identification of metabolic and ultrastructural changes to the kidney following ischemia-reperfusion injury. *Am. J. Physiol. Ren. Physiol.* **314**, F154–F166 (2018).
 46. Yang, X., Wu, H. & Li, H. Dehydration-associated chronic kidney disease: a novel case of kidney failure in China. *BMC Nephrol.* **21**, 159 (2020).
 47. Stefanidis, I. et al. Association between heparan sulfate proteoglycan excretion and proteinuria after renal transplantation. *J. Am. Soc. Nephrol.* **7**, 2670–2676 (1996).
 48. Halimi, J. M. et al. Early low-grade proteinuria: causes, short-term evolution and long-term consequences in renal transplantation. *Am. J. Transpl.* **5**, 2281–2288 (2005).
 49. Artz, M. A., Dooper, P. M., Meuleman, E. J., van der Vliet, J. A. & Wetzels, J. F. Time course of proteinuria after living-donor kidney transplantation. *Transplantation* **76**, 421–423 (2003).
 50. Youle, R. J. & Karbowski, M. Mitochondrial fission in apoptosis. *Nat. Rev. Mol. Cell Biol.* **6**, 657–663 (2005).
 51. Szeto, H. H. et al. Mitochondria protection after acute ischemia prevents prolonged upregulation of IL-1. *J. Am. Soc. Nephrol.* **28**, 1437–1449 (2017).
 52. Machiela, E. et al. Disruption of mitochondrial dynamics increases stress resistance through activation of multiple stress response pathways. *FASEB J.* **34**, 8475–8492 (2020).
 53. Fukumitsu, K. et al. Synergistic action of dendritic mitochondria and creatine kinase maintains ATP homeostasis and actin dynamics in growing neuronal dendrites. *J. Neurosci.* **35**, 5707–5723 (2015).
 54. Boyer, O., Mollet, G. & Dorval, G. Neurological involvement in monogenic podocytopathies. *Pediatr. Nephrol.* **36**, 3571–3583 (2021).
 55. Denic, A. et al. Glomerular volume and glomerulosclerosis at different depths within the human kidney. *J. Am. Soc. Nephrol.* **30**, 1471–1480 (2019).
 56. Altintas, M. M. et al. Reduction of proteinuria through podocyte alkalinization. *J. Biol. Chem.* **289**, 17454–17467 (2014).
 57. Asano, T. et al. Permanent genetic tagging of podocytes: fate of injured podocytes in a mouse model of glomerular sclerosis. *J. Am. Soc. Nephrol.* **16**, 2257–2262 (2005).
 58. Kisanuki, Y. Y. et al. Tie2-Cre transgenic mice: a new model for endothelial cell-lineage analysis in vivo. *Dev. Biol.* **230**, 230–242 (2001).
 59. Endo, T. et al. Exploring the origin and limitations of kidney regeneration. *J. Pathol.* **236**, 251–263 (2015).
 60. Cui, M. et al. Mdivi-1 protects against ischemic brain injury via elevating extracellular adenosine in a cAMP/CREB-CD39-dependent manner. *Mol. Neurobiol.* **53**, 240–253 (2016).
 61. Mundel, P., Reiser, J. & Kriz, W. Induction of differentiation in cultured rat and human podocytes. *J. Am. Soc. Nephrol.* **8**, 697–705 (1997).
 62. Mundel, P. et al. Rearrangements of the cytoskeleton and cell contacts induce process formation during differentiation of conditionally immortalized mouse podocyte cell lines. *Exp. Cell Res* **236**, 248–258 (1997).
 63. Lysenkova, L. N. et al. Verification of oligomycin a structure: synthesis and biological evaluation of 33-dehydrooligomycin A. *J. Antibiot. (Tokyo)* **70**, 871–877 (2017).
 64. Gu, L. et al. Low dose of 2-deoxy-D-glucose kills acute lymphoblastic leukemia cells and reverses glucocorticoid resistance via

- N-linked glycosylation inhibition under normoxia. *Oncotarget* **8**, 30978–30991 (2017).
65. Sano, T. et al. Intravital imaging of mouse urothelium reveals activation of extracellular signal-regulated kinase by stretch-induced intravesical release of ATP. *Physiol Rep* **4**, e13033 (2016).
 66. Buval, L. et al. Proteasomal degradation of Nck1 but not Nck2 regulates RhoA activation and actin dynamics. *Nat. Commun.* **4**, 2863 (2013).
 67. Zhong, F., Wang, W., Lee, K., He, J. C. & Chen, N. Role of C/EBP- α in Adriamycin-induced podocyte injury. *Sci. Rep.* **6**, 33520 (2016).
 68. Mallipattu, S. K. et al. Expression of HIV transgene aggravates kidney injury in diabetic mice. *Kidney Int* **83**, 626–634 (2013).
 69. Guan, N. et al. Protective role of cyclosporine A and minocycline on mitochondrial disequilibrium-related podocyte injury and proteinuria occurrence induced by adriamycin. *Nephrol. Dial. Transpl.* **30**, 957–969 (2015).
 70. Ichimura, K. et al. Morphological processes of foot process effacement in puromycin aminonucleoside nephrosis revealed by FIB/SEM tomography. *J. Am. Soc. Nephrol.* **30**, 96–108 (2019).
 71. Belevich, I., Joensuu, M., Kumar, D., Vihinen, H. & Jokitalo, E. Microscopy image browser: a platform for segmentation and analysis of multidimensional datasets. *PLoS Biol.* **14**, e1002340 (2016).
 72. Hall, A. M., Unwin, R. J., Parker, N. & Duchon, M. R. Multiphoton imaging reveals differences in mitochondrial function between nephron segments. *J. Am. Soc. Nephrol.* **20**, 1293–1302 (2009).
 73. Lindsey, M. L. et al. Guidelines for experimental models of myocardial ischemia and infarction. *Am. J. Physiol. Heart Circ. Physiol.* **314**, H812–H838 (2018).
 74. Weinberg, J. M., Venkatachalam, M. A., Roeser, N. F. & Nissim, I. Mitochondrial dysfunction during hypoxia/reoxygenation and its correction by anaerobic metabolism of citric acid cycle intermediates. *Proc. Natl Acad. Sci. USA* **97**, 2826–2831 (2000).
 75. Bajwa, A. et al. Sphingosine 1-phosphate receptor-1 enhances mitochondrial function and reduces cisplatin-induced tubule injury. *J. Am. Soc. Nephrol.* **26**, 908–925 (2015).
 76. Kanda, Y. Investigation of the freely available easy-to-use software 'EZR' for medical statistics. *Bone Marrow Transpl.* **48**, 452–458 (2013).

Acknowledgements

We thank Professor Peter Mundel for kindly providing us with the murine podocyte cell line. We thank Dr. Spyros Goulas for critical reading and constructive suggestions on our paper. We thank Professor János Peti-Peterdi for technical instructions. We also thank Division of Electron Microscopic Study, Center for Anatomical Studies, Graduate School of Medicine, Kyoto University for technical assistance in electron microscopy. This research was supported by the Japan Agency for Medical Research and Development (AMED) under Grant Number AMED-CREST 22gm1210009, 22gm5010002, 22zf0127003h001, and 22ek0310020h0001 (to MoY) and by KAKENHI Grant-in-Aids for Scientific Research B (20H03697 (to MoY) and 21K16162 (to ShinY)). This work was partly supported by the World Premier International Research Center Initiative (WPI), MEXT, Japan. Part of this work appeared as an abstract at the annual meeting of the American Society of Nephrology. This work was also supported by Platform for Drug Discovery, Informatics, and Structural Life Science from the Ministry of Education, Culture, Sports, Science and Technology, Japan and by Kyoto University Live Imaging Center and in part by Grants-in-Aid KAKENHI 16H06280 "ABiS". This work was also partly supported by the Mochida Memorial Foundation for Medical and Pharmaceutical Research, Japan, Suzuken Memorial Foundation, Japan, and Gout and Uric Acid Foundation of Japan.

Author contributions

M.T. and Mo.Y. designed the experiments. M.T., S.Y., and Mo.Y. wrote the manuscript. Mo.Y. supervised the project. M.T. performed the experiments and collected and analyzed the data. S.F. supervised statistical

analyses. S.Y., A.O., Y.N., K.K., T.M., Ma.Y., and M.M. and other authors discussed the results and commented on the manuscript.

Competing interests

MoY has received research grants from Mitsubishi Tanabe Pharma Corp. and Boehringer Ingelheim Co., LTD. MaY has received research grants from Meiji Holdings and Boehringer Ingelheim Co., LTD. and holds patents (JP6593595, US11160879). ShigY was employed by the TMK Project, which was a collaborative project between Kyoto University and Mitsubishi Tanabe Pharma Corp. KK has received lecture fees from Astellas Pharma Inc., AstraZeneca K.K., MSD K.K., Otsuka Pharmaceutical Co., Ltd., Ono Pharmaceutical Co., Ltd., Kyowa Kirin Co., Ltd., Kowa Co., Ltd., Sanofi K.K., Sumitomo Dainippon Pharma Co., Ltd. (Sumitomo Pharma Co., Ltd.), Mitsubishi Tanabe Pharma Corp., Eli Lilly Japan K.K., Nippon Boehringer Ingelheim Co., Ltd., Novartis Pharma K.K., Novo Nordisk Pharma Ltd., Bayer Yakuhin, Ltd., Pfizer Japan Inc., and Janssen Pharmaceutical K.K.; funded research or joint research expenses from Kowa Co., Ltd., AstraZeneca K.K., Daiichi Sankyo Co., Ltd., Novo Nordisk Pharma Ltd., Amgen, Janssen Pharmaceutical K.K., Parexel International Inc., and Astellas Pharma Inc. His affiliated institution (Shinshu University School of Medicine) has received grants from Otsuka Pharmaceutical Co., Ltd., Mitsubishi Tanabe Pharma Corp., Nippon Boehringer Ingelheim Co., Ltd., and Kyowa Kirin Co., Ltd., and his department has endowed chairs from Medtronic Japan Co., Ltd., Boston Scientific Japan K.K., Abbott Japan LLC, Japan Lifeline Co., Ltd., Biotronik Japan, Terumo Corporation, Nipro Corporation, and Cordis Japan G.K. The other authors declare no conflicts of interest.

Additional information

Supplementary information The online version contains supplementary material available at <https://doi.org/10.1038/s41467-024-54222-0>.

Correspondence and requests for materials should be addressed to Motoko Yanagita.

Peer review information *Nature Communications* thanks Francesco Di Virgilio, Alla Mitrofanova and the other, anonymous, reviewer(s) for their contribution to the peer review of this work. A peer review file is available.

Reprints and permissions information is available at <http://www.nature.com/reprints>

Publisher's note Springer Nature remains neutral with regard to jurisdictional claims in published maps and institutional affiliations.

Open Access This article is licensed under a Creative Commons Attribution-NonCommercial-NoDerivatives 4.0 International License, which permits any non-commercial use, sharing, distribution and reproduction in any medium or format, as long as you give appropriate credit to the original author(s) and the source, provide a link to the Creative Commons licence, and indicate if you modified the licensed material. You do not have permission under this licence to share adapted material derived from this article or parts of it. The images or other third party material in this article are included in the article's Creative Commons licence, unless indicated otherwise in a credit line to the material. If material is not included in the article's Creative Commons licence and your intended use is not permitted by statutory regulation or exceeds the permitted use, you will need to obtain permission directly from the copyright holder. To view a copy of this licence, visit <http://creativecommons.org/licenses/by-nc-nd/4.0/>.

© The Author(s) 2024